AFOSR-TR-97

0519

REPORT DOCUMENTATION PAGE

1. AGENCY USE ONLY (Leave blank)	2. REPORT DATE	3. REPORT TYPE AND DATES COVERED
	9/26/97	Final Technical - 8/1/94-4/14/97

4. TITLE AND SUBTITLE
Ceramics from Metal-Organic Precursors

5. FUNDING NUMBERS
F49620-95-1-0011
2303/BS
61102F

6. AUTHOR(S)
Donald R. Uhlmann, Professor

7. PERFORMING ORGANIZATION NAME(S) AND ADDRESS(ES)
Department of Materials Science and Engineering
The College of Engineering and Mines
The University of Arizona
Tucson, AZ 85721

8. PERFORMING ORGANIZATION REPORT NUMBER

9. SPONSORING / MONITORING AGENCY NAME(S) AND ADDRESS(ES)
AFOSR/NL
110 Duncan Avenue Suite B115
Bolling AFB, DC 20332-0001

10. SPONSORING / MONITORING AGENCY REPORT NUMBER

11. SUPPLEMENTARY NOTES

12a. DISTRIBUTION / AVAILABILITY STATEMENT
Approved for Public Release
Distribution is Unlimited

19971021 246 DTIC

13. ABSTRACT (Maximum 200 words)

Our efforts during the past year, as outlined in the proposal, have been on the improvement in photostability of laser dyes within sol-gel derived hosts through the understanding of the dye/matrix interactions. The efforts of the research program can be best described by the manuscripts that have been or are being published. These manuscripts are included in the present progress report.

14. SUBJECT TERMS

15. NUMBER OF PAGES
6

16. PRICE CODE

17. SECURITY CLASSIFICATION OF REPORT	18. SECURITY CLASSIFICATION OF THIS PAGE	19. SECURITY CLASSIFICATION OF ABSTRACT	20. LIMITATION OF ABSTRACT
UNCLASSIFIED	UNCLASSIFIED	UNCLASSIFIED	UNLIMITED

FINAL TECHNICAL REPORT

on

CERAMICS FROM METAL-ORGANIC PRECURSORS

submitted to

AIR FORCE OFFICE OF SCIENTIFIC RESEARCH

by

THE UNIVERSITY OF ARIZONA

TUCSON, AZ 85721

GRANT: F49620-95-1-0011

August 1, 1994 - April 14, 1997

Professor Donald R. Uhlmann
Principal Investigator

Final Technical Report 1997

Our efforts during the past year, as outlined in the proposal, have been on the improvement in photostability of laser dyes within sol-gel derived hosts through the understanding of the dye/matrix interactions. The efforts of the research program can be best described by the manuscripts that have been or are being published. These manuscripts are included in the present progress report.

The development of a tunable solid-state laser in the visible has been the object of extensive research during the past decade. Fluorescent organic dyes within solid hosts represent attractive materials for use in such applications; but the lack of photostability has been a major factor limiting their commercial use. Today, commercial laser dyes typically pump a dye solution through a resonator and suffer from limited lifetime due to photodecomposition and chemical instability as well as inherent problems with pumping and with the use of solvent systems. Incorporating fluorescent dyes within a solid host should reduce these problems, and can provide low cost lasers which are tunable over the entire visible spectrum. Because of the large absorption bandwidth of laser dyes, such systems can be pumped

with a flash lamp, eliminating the need for laser pumping and reducing system cost and space. It is recognized that solid state dye lasers would have numerous applications, at both low and high power levels, in the medical and defense industries.

The thrust of the present research program is to find ways to improve the photostability of laser dyes within sol-gel hosts through molecular engineering techniques. These techniques are best summarized by the paper "Molecular Engineering and Photostability of Laser Dyes within Sol-Gel Hosts" (Solid State Lasers VI, SPIE vol. 2986, pages 141-152) which is enclosed with this document. The techniques that were successfully utilized to improve photostability include: covalently attaching the laser dye to the host; controlling the chemical environment of the dye; increasing dye caging by increasing the SiO_2 content; removing porosity from the host; and incorporating additives to minimize photodegradation.

One of the techniques listed above, removing porosity from the host, is described in greater detail in "Control of Porosity in SiO_2:PDMS Polycerams through Variations in Sol-Gel Processing and Polymer Content" (to appear in Sol-Gel Optics IV, SPIE 1997). The removal of porosity reduces the ability for oxygen to diffuse to the dye molecule and cause

photodegradation. This paper discusses how porosity control is actually achieved from a chemistry/materials science point of view during processing of the Polycerams. The key to the control of the porosity is through the variation of the relative rates of condensation and evaporation during processing.

Another one of the techniques described above, control of the chemical environment, was taken a step further in the paper "Reversing Gels and Water Soluble Colloids from Aminosiloxanes" (to be published in Journal of Sol-Gel Science and Technology). It was found that to prevent chemical degradation of the Pyrromethene laser dye, a basic environment was required. A new host composition that provided a basic environment, synthesized from aminosiloxanes, provided significant improvement in photostability. This new host composition, also had some unique properties (e.g., reversible gelation, water solubility) which are explored in greater detail this manuscript.

To summarize the work of the past year, significant improvement in the photostability of laser dyes with sol-gel hosts has been achieved. This was accomplished by first examining the mechanism by which these laser

dyes degrade and then by utilizing molecular engineering techniques to prevent photodegradation processes from occurring.

Reversing Gels and Water Soluble Colloids from Aminosiloxanes

T. Suratwala, K. Davidson, Z. Gardlund, D. Collins, and D.R. Uhlmann
Department of Materials Science and Engineering,
Arizona Materials Laboratory, University of Arizona
4715 E. Fort Lowell, Tucson, AZ 85712

The unique sol/gel behavior of an organic/inorganic hybrid material synthesized from 3-aminopropyltriethoxysilane (3AS) and tetramethoxysilane (TMOS) is discussed and examined. The addition of H_2O to a mixture of a basic (3AS) and an acidic (TMOS) alkoxide leads to rapid gel formation. This wet gel reverses to a sol upon heating which is attributed to the dissolution of siloxane bonds between the surfaces of colloidal particles in the gel. The reversed sol dries to an optically transparent solid which is water soluble. The water solubility and the stability of these colloidal particles are described by their aminopropyl/silanol surface and the electrostatic interactions between them using DLVO theory.

Keywords: water soluble silica, colloids, 3-aminopropyltriethoxysilane, tetramethoxysilane, reversible gel, DLVO theory

1. Introduction

The gelation of colloidal silica can be pictured as the collision between colloids with silanol surfaces resulting in condensation reactions to form siloxane bonds. The siloxane bonds are formed irreversibly, and the resulting gel/precipitate is water-insoluble. Silica gels can be made water soluble: (1) by including substituents in the composition which prevent siloxane bond formation or (2) by placing the material in a highly basic environment where dissolution of the siloxane bonds can take place. Alkali metal silicates such as Na and K silicates[1] and certain organically modified sols are known to be water soluble[1, 2]. At a high pH, the silica surface will have a negative surface charge, and the positive cations (Na, K, Li, etc.) will adsorb on the surface of silica. Particles will then be linked together by acid-base bonds rather than siloxane bonds, and these materials can be peptized to become water soluble[1]. Organically

modified sols can also be water soluble by incorporating organic ions on the surface of the silica such as tetramethylammonium ions[1, 3, 4], again preventing siloxane bond formation.

In this study, we present a new organically modified silicate material and discuss its unique characteristics of reversible gelation and water solubility which is believed to be governed by the dissolution of silica and electrostatic interactions between silica colloids.

2. Experimental

Synthesis. The physical behavior of the 3AS:TMOS composition during processing is shown in Fig. 1. Typically, 3AS, TMOS, and H_2O (distilled or acidified) were mixed in a vial at a 5.5:1:3.9 mole ratio. Upon the addition of H_2O, rapid hydrolysis/condensation resulted in the formation of a wet gel (B) within 60 seconds of mixing with distilled H_2O and within 10 seconds of mixing with acidified H_2O. This wet gel (B) was optically transparent, often with a bluish color caused by Raleigh scattering. Upon heating the wet gel to 75 C for several hours, the gel would reverse back to an optically transparent solution (C). The reversed solution (C) was slightly more viscous than the original 3AS:TMOS solution (A). Solution (C) was very stable, since it would not gel upon sitting. The drying of solution (C) resulted in an optically transparent, crack free solid (D). The addition of water to the solid (D) returned the solid to a solution (C). The rate of dissolution was slow; it typically took several hours at 75 C.

Atomic Force Microscopy (AFM). The reversed solutions (C) were diluted in water and deposited and dried on mica. Images were taken in tapping mode on a Nanoscope III (Digital Instruments) AFM.

3. Results and Discussion

The formation of the wet gel (B) can be explained by examining the acid/base catalysis of the sol-gel reactions. As individual precursors, TMOS and 3AS hydrolyze rapidly within 30 sec in the presence of water. Just after hydrolysis, these solutions are fluid, and do not form a gel as in the presently-studied (mixed) system. During typical

sol-gel processing, treating an alkoxide in a acidic environment catalyzes both the hydrolysis and condensation reactions. The hydrolysis rate typically far exceeds the condensation rate, resulting in relatively long gel times[1, 5]. As the pH increases, the condensation rate increases, decreasing the gel time. 3AS is an alkoxide with a basic amine substituent, while TMOS is a relatively acidic alkoxide. The addition of H_2O to a mixture of an acid and a basic alkoxide results in rapid gel formation which is attributed to rapid catalysis of both hydrolysis (due to the acidic TMOS) and condensation (due to the basic 3AS).

The high optical transparency of the wet gel (B) suggests the rates of hydrolysis and condensation of the two alkoxides are closely matched and hence both of the alkoxides are being homogeneously incorporated into the matrix. By comparison, when H_2O is added to a mixture of tetraethoxysilane (TEOS) and 3AS, or to a mixture of TMOS and 3-aminopropyltrimethoxysilane (3AMS), a precipitate is formed, suggesting that the reaction rates of the two alkoxides are not matched. The hydrolysis/condensation rate of TEOS is much slower than that of TMOS and the reaction rate of 3AMS is faster than that of 3AS[5, 6]. However, when water is added to TMOS and 4-aminobutyltriethoxysilane, which should have similar reaction rates as 3AS, an optically transparent initial gel is formed that behaves like the 3AS:TMOS compositon.

The wet gel (B) reverses to a solution which contains colloidal particles (i.e., forms a sol); an AFM image of the colloidal particles (10-15 nm in diameter) is shown in Fig. 2a for a compositon at 3AS:TMOS=5.5. The gel-to-sol transition is likely caused by the dissolution of the siloxane crosslinks (i.e., the break up of Si-O-Si bonds by hydrolysis or reesterification reactions where solvent has easy access). The solubility of silica is known to increase at high pH [1, 5], and the large amine concentration in the present composition makes the gel very basic (pH=9-10). Also, silica solubility increases by a factor of three upon increase in temperature from 25 C to 75 C[1], which coincides with the fact that the wet gel reversal rate increases with temperature.

One could argue that the wet gel (B) is being held together by hydrogen bonds through the amine groups and the silanol groups between the colloids, and the increase (decrease) in temperature causes the break up (formation) of these bonds. However, gel

(B) was only one-time reversing (i.e., solution (C) did not gel upon cooling). Hence hydrogen bond breakage is likely not the source of the reversal. Another reason which suggests that hydrogen bonds are not playing a role is the fact that solid (D) does not become fluid upon heating. Rather, the solid (D) goes into solution only upon the addition of a solvent such as water.

The addition of different solvents in solution (A) provides some further evidence that dissolution of the silica is occurring during the gel-to-sol transition. Ethanol (EtOH) was added to the 3AS:TMOS mixture (A), and a gel was still formed when water was added. The ethanol containing gels still reversed and behaved like compositions without added solvent (Fig. 1). In contrast, 3AS:TMOS solutions in tetrahydrofuran (THF), also form an optically transparent gel (B), but the gels were found to be irreversible. Protic solvents, such as EtOH, can hydrogen bond to hydroxl ions or siloxanes to make them more electrophilic and can influence the reverse reactions as shown below[5]:

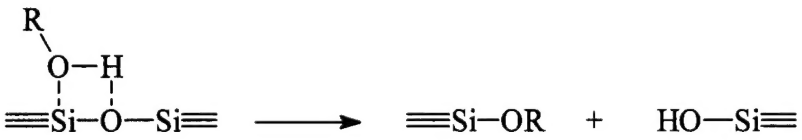

Aprotic solvents, such as THF or dioxane, are considerably more inert. They cannot hydrogen bond to hydroxyl ions (or siloxanes) and cannot participate in the hydrolysis or reesterification of siloxane bonds. This supports the suggestion that the wet gel (B) formation is due to siloxane crosslinking as opposed to just hydrogen bonding, and the gel-to-sol reversal is due to the dissolution of silica.

A phase diagram for the 3AS+TMOS+H_2O system determined as a function of the acid content and the 3AS:TMOS ratio gives insight into the behavior of the gel (Fig. 3). In all cases, except at a 3AS:TMOS ratio of ∞, a wet gel (B) was formed. At lower acid contents and lower TMOS contents, the wet gels (B) were reversible. As the acid content increases, the degree of hydrolysis/ condensation of the alkoxides increases, thereby, increasing the number of crosslinks between the colloidal particles. High crosslink densities decreases the ability for dissolution to cause breakup of the colloids and to cause gel reversal to a sol. As the TMOS content increases, the number of crosslink sites between the colloids should also increase, because TMOS is four functional and the 3AS

is only 3 functional. At very high TMOS contents (3AS:TMOS < 2), the wet gel (B) did not reverse.

The reversed solutions (B) became more viscous with increasing TMOS content. This is believed to be caused by the increase in the colloid size and colloid interaction at higher TMOS contents as indicated by the AFM images in Fig. 2. At a 3AS:TMOS=5.5:1 (Fig. 2a), the dispersed colloid size was relatively small (10-15 nm), while at 3AS:TMOS=3:1 (Fig. 2c), the size was much larger (40-100 nm). There was also greater interaction between the colloids at 3AS:TMOS=3:1, because at higher colloid concentrations, the colloid size increases dramatically (Fig. 2d). In contrast, with the 3AS:TMOS=5.5:1 composition, the colloid size does not increase as much (Fig. 2b). The greater interaction between the colloids of the higher TMOS samples could stem from the larger concentrations of silanols at the surface which can undergo condensation reactions (i.e., there are fewer amine groups to block the surface silanols).

3AS alone hydrolyzed by H_2O is unusually stable in aqueous environments[7]. The unique water solubility stems from the formation of low molecular weight cage structures and from internal cyclization, where the propyl amine group wraps around and hydrogen bonds with the silanol groups[7, 8]. The propyl amine in this configuration blocks the silanol groups and hinders the condensation reactions, resulting in high stability in aqueous environments. The energy for cyclization has been reported to be -26.3 kcal/mole, which is much greater than the thermal energy[7]. When both 3AS and TMOS are hydrolyzed together, larger cage structures (colloids) are believed to be formed which are linked mostly by siloxane bonds in the wet gel (B). After dissolution, the reversed solution (C) does not return to a gel (B) upon cooling because: (1) the internal cyclization of the amine groups to the silanol groups on the surface of the colloids hinders inter-colloid condensation; and (2) the electrostatic interactions between the colloids contributes to the colloid-colloid repulsion (see discussion below). For these same reasons, the dried gel (D) is water soluble (see Fig. 4).

Two experiments confirm that the interaction of the colloidal particles is governed by electrostatic forces. First, the colloidal solution (B) precipated when $ZrCl_4$ was added to the solution. The addition of a multivalent salt contributed to the decrease in the

electrical double layer and hence caused flocculation or coagulation. Second, the particles have a significant zeta potential of -30 to -40 mV as measured by electrophoresis, suggesting that a strong surface charge exists on the colloids.

Knowing this, Derjaguin-Landau-Verwey-Overbeek (DLVO) theory can be applied to confirm and predict conditions under which flocculation or dispersion of the colloids will occur[9]. DLVO theory takes into account electrostatic repulsion and van der Waals attraction and can be described by:

$$\kappa = \left[\left(\frac{4\pi}{\varepsilon\,\varepsilon_0\,k_B\,T}\right)\cdot\left[n_p\,Z_p{}^2\,e^2 + n_\alpha\,Z_\alpha{}^2\,e^2\right]\right]^{\frac{1}{2}}$$

$$U_A = -\frac{A}{6}\cdot\left(\frac{2\,a_p{}^2}{r^2 - 4\,a_p{}^2} + \frac{2\,a_p{}^2}{r^2} + \ln\left(\frac{r^2 - 4\,a_p{}^2}{r^2}\right)\right)$$

$$U_R = \frac{Z^2\,e^2}{\varepsilon\,\varepsilon_0}\cdot\left(\frac{\exp(\kappa\,a_p)}{1+\kappa\,a_p}\right)\cdot\frac{\exp(-\kappa\,r)}{r}$$

$$U_T = U_A + U_R$$

where κ^{-1} is the screening length (approximately the double layer thickness), U_R is the Columbic repulsion energy, U_A is the van der Waals attraction energy, ε is the dielectric constant of the solvent, ε_0 is the permittivity of a vacuum, k_B is Boltzmann's constant, T is the temperature, n_p is colloid density, Z_p is valence of colloidal particle, e is the charge of an electron, n_α is the counterion density, Z_α is the counterion valence, a_p is the particle radius, r is the distance between particles, and A is the Hamaker constant[9].

The reversed solution (C) was added to a variety of different solvents. In general, high dielectric solvents resulted in a stable colloid mixture, while low dielectric constant solvents result in flocculation of the colloidal particles. A decrease in the dielectric constant results in the decrease in the electrical double layer, and hence causes flocculation. Fig. 5 is a plot of the energy between two colloids relative to the thermal energy for three solvents (H_2O (ε=78), EtOH (ε=24), and benzene (ε=2)) as a function of the distance between the colloids in units of particle diameter as predicted by DLVO theory. The low dielectric constant solvent, benzene, has a minumum in the energy curve suggesting that the colloids should flocculate; the curves for the two other solvents do not

have an energy minimum, suggesting that the particles should be dispersed. The predicted behavior in Fig. 5 matched the experimental results of adding the respective solvents, and therefore the behavior of the 3AS:TMOS colloids seems well predicted by DLVO theory.

4. Conclusions

A sol-gel material derived from 3AS and TMOS prcursors has been characterized, and its unique properties of reverible gelation and water solubility have been described. The reversibility of the initial gel is caused by the dissolution of the Si-O-Si in the presence of a highly basic environment. This results in formation of colloidal particles with amine and silanol surfaces that are water soluble, and whose behavior is governed by electrostatic interactions.

5. Acknowledgments

The financial support of the Air Force Office of Scientific Research is gratefully acknowledged.

References

1. R. Iler, *The Chemistry of Silica* (John Wiley & Sons, New York, 1979).
2. J. Vail, *Soluble Silicates*, ACS Monograph Series (Reinhold, New York, 1952), vol. 1 & 2.
3. R. Iler, U.S. Patent 2,692,863 (Dupont, 1954).
4. D. Shaefer, U.S. Patent 3,625,856 (Nalco Chemical Co., US, 1971).
5. C. Brinker, G. Scherer, *Sol-Gel Science* (Academic Press, Inc., Boston, 1990).
6. H. Schmidt, H. Scholze, A. Kaiser, *Journal of Non-Crystalline Solids* **63**, 1-11 (1984).
7. E. Plueddemann, *Silane Coupling Agents* (Plenum Press, New York, 1982).
8. C. Chiang, H. Ishida, J. Koenig, *74* **2**, 396 (1980).
9. A. Sood, in *Solid State Physics* (Academic Press, 1991), vol. 45, pp. 1-73.
10. J. Israelachvili, *Intermolecular & Surface Forces* (Academic Press Limited, San Diego, 1992).

Fig. 1. Schematic of the physical behavior of the 3AS:TMOS composition during processing.

Fig. 2. AFM images of diluted reversed solutions with (a) 3AS:TMOS=5.5 at low concentrations (b) 3AS:TMOS=5.5 at higher concentrations (c) 3AS:TMOS=3 at low concentrations (d) 3AS:TMOS=3 at higher concentrations. The full scale for each image is 1000 nm.

Fig. 3. Phase diagram of 3AS:TMOS compositions as a function of H_2SO_4 content and TMOS content.

Fig. 4. Schematic representation of the colloidal particles and possible colloid-colloid interactions present in the 3AS:TMOS system in the initial gel (B), reversed solution (C), and in the solid dried gel (D).

Fig. 5. Interaction energy of two colloidal particles relative to the thermal energy predicted by DLVO theory (a) upon change in the dielectric constant of the solvent (for water ε=78 $A=0.323*10^{-20}$ joule, for ethanol ε=26 and $A=0.181*10^{-20}$ joule, for benzene ε=2 and $A=0.373*10^{-20}$ joule) with the parameters Z_p=2500, a_p=6 nm, T=300K, $n_p=10^{17}$ cm^{-3}, and $n_\alpha=Z*n_p$. Hamaker constants were estimated using equation 11.14 from Israelachvili[10].

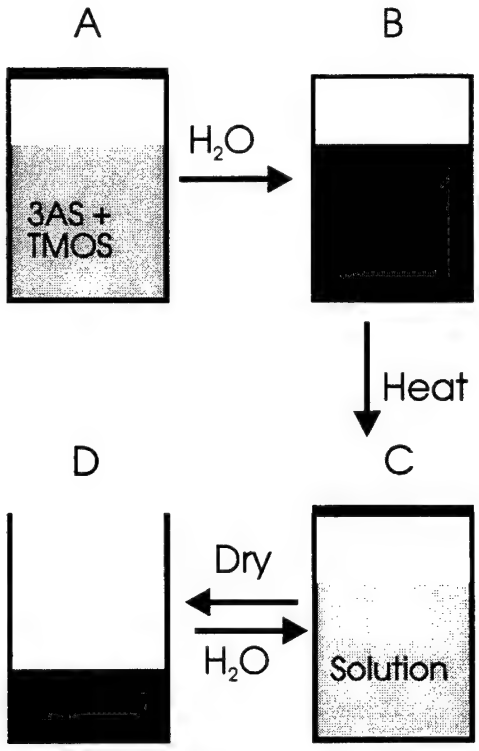

Fig. 1.

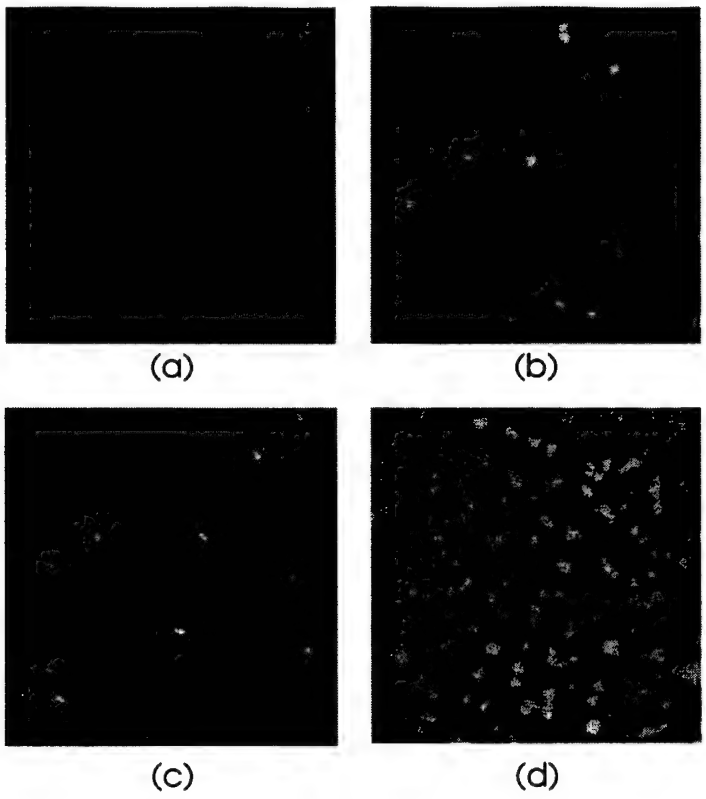
(a)
(b)
(c)
(d)

Fig. 2.

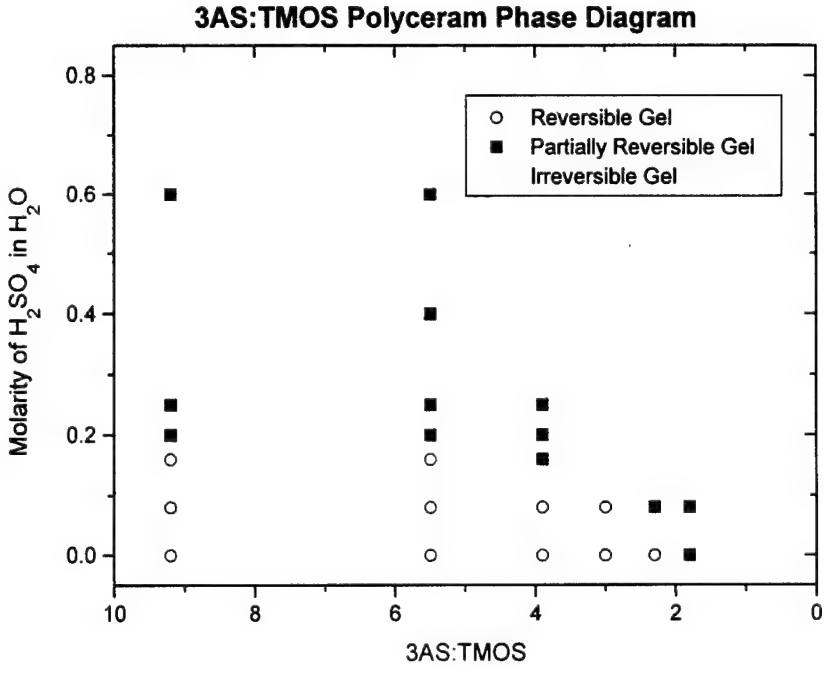
3AS:TMOS Polyceram Phase Diagram
Reversible Gel
Partially Reversible Gel
Irreversible Gel
Molarity of H_2SO_4 in H_2O
0.0
0.2
0.4
0.6
0.8
10
8
6
4
2
0
3AS:TMOS

Fig. 3.

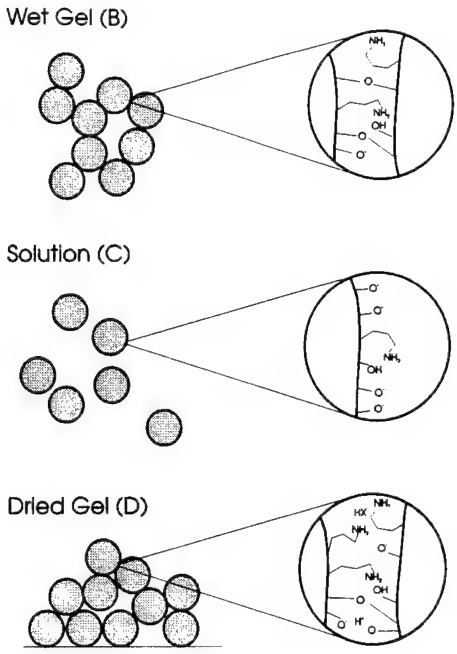
Wet Gel (B)
Solution (C)
Dried Gel (D)

Fig. 4.

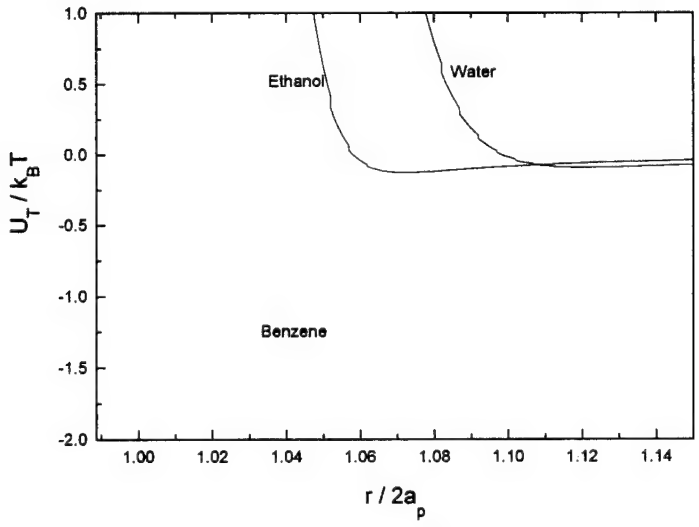
Ethanol
Water
Benzene
$U_T / k_B T$
$r / 2a_p$
1.0
0.5
0.0
-0.5
-1.0
-1.5
-2.0
1.00
1.02
1.04
1.06
1.08
1.10
1.12
1.14

Fig. 5.

Molecular Engineering and Photostability of Laser Dyes within Sol-Gel Hosts

T. Suratwala, K. Davidson, Z. Gardlund, and D.R. Uhlmann

Department of Materials Science and Engineering, Arizona Materials Laboratory
University of Arizona, 4715 E. Fort Lowell, Tucson, AZ 85712, USA

S. Bonilla and N. Peyghambarian

Optical Sciences Center, Meinel Building, University of Arizona, Tucson, AZ 85721, USA

ABSTRACT

The use of a solid-state dye laser for commercial applications has been limited largely by the poor photostability of the gain medium. Techniques are examined to improve the photostability of Coumarin and Pyrromethene-BF_2 567 (PM-567) laser dyes within xerogel and Polyceram hosts synthesized by sol-gel processing. The photochemical mechanisms by which laser dyes degrade are discussed and determined specifically for PM-567. PM-567 was determined to degrade both by photo-oxidation and acid degradation. Techniques for improving photostability are described from a molecular engineering perspective. These techniques include: covalently attaching the laser dye to the host; controlling the chemical environment of the dye; increasing dye caging by increasing the SiO_2 content; removing porosity from the host; and incorporating additives such as hindered amine light stabilizers to minimize photodegradation.

Keywords: Pyrromethene-BF_2 567, Solid-State Dye Laser, Sol-Gel, Polycerams, Photostability, Antioxidants, Porosity, Polydimethylsiloxane

1. INTRODUCTION

Lasing can take place in a variety of media, including solids, liquids, gases, and even plasmas. Liquid dye lasers are important because of their large wavelength tunability in the visible, low threshold powers, and pump source flexibility. Many families of lasing dyes exist such as Coumarins, Rhodamines, and Pyrromethenes. Most commercial lasing dyes are dissolved at low concentrations of 10^{-3} to 10^{-4} M in solvents (alcohols, H_2O or ethylene glycol). Flow of the dye/solvent mixture through the resonator chamber is required to maintain photostability. This allows the dye molecules to move in and out of the pump beam within the resonator, giving the excited dye molecules time to return to ground state and minimizing dye degradation.

In the last several decades there has been much interest in developing a solid-state dye laser. The dye/solvent laser system requires fluid pumping devices, and therefore a solid-state medium would be a good alternative. A solid-state gain medium would avoid problems associated with dye/solvent systems, such as convection, evaporation, flow fluctuations, solvent poisoning, and dye poisoning [1], and would provide ease of use and replacement, along with expanded applications as slab waveguide lasers, tunable fiber-optic lasers, and solid-state dye laser rods. Dye/host interactions could also enhance control of the fluorescence spectra, improve the quantum efficiency of fluorescence, and even improve photostability.

A tunable solid-state laser would have numerous applications in medicine. Currently, liquid dye lasers have potential use in dermatology for the removal of vascular lesions, in cardiology for the break up of blood clots, and in urology for the break up of urinary stones[2-6]. In the past ten years, the use of lasers in surgical and medical practices has increased; this market desires improved wavelength agility, low cost, and compactness of the laser system. A photostable solid-state laser could provide all of these. The output of multiple wavelengths not only allows for selective heating by preferential light absorption by the target material (e.g., oxyhemoglobin, de-oxyhemoglobin, melanin, various tattoo ink pigments), but also allows for different penetration depths of the laser light. The low cost and compactness stems from the simplicity of the laser system; solid-state dye lasers would not require fluid pumping devices, and flashlamp pumping as opposed to laser pumping can be used, which decreases the cost and size of the laser system.

Dyes have been incorporated within a variety of solid-state hosts such as polymers, porous glasses, low temperature glasses, and sol-gel derived glasses in which low processing temperatures are used to prevent thermal degradation of the dye. Poor photostability of the dye within the host has been the major limitation of these materials. Enhancement in photostability can be achieved by optimizing the laser system design, by synthesizing a more photostable laser dye, and by controlling dye/host interactions in the gain medium. Utilizing the last method, dye/host interactions are examined for Coumarin and PM-567 dyes within sol-gel derived xerogels (air dried porous gels) and Polycerams (polymer-modified ceramic materials in which the organic and inorganic components are combined on a near-molecular scale). Polycerams are attractive hosts because they provide optically transparent, polishable monoliths, and because the physical properties of the host and dye/host interactions can be controlled through variations in processing and composition.

In this study, we will consider the mechanisms by which lasing dyes degrade, specifically for PM-567. Then a series of molecular engineering techniques, involving control of dye/host interactions which lead to improved photostability of the dye/host system, are discussed. These techniques can be used for the design and synthesis of dye/host laser materials requiring high photostability as well as other dye/host materials in which high photostabilities are desired such as those containing photochromic dyes, nonlinear optic dyes, coloring dyes, and chemical sensing dyes.

2. EXPERIMENTAL

Material Synthesis. SiO_2 xerogel and SiO_2:Polydimethylsiloxane (PDMS) Polyceram hosts were doped with Coumarin and Pyrromethene dye using the sol-gel process. Details of the dye synthesis and sol-gel processing are described elsewhere[7, 8]. As an example, one of the synthetic routes used to synthesize PM-567 doped SiO_2:PDMS Polycerams is shown schematically in Figure 1. The resulting Polycerams were optically transparent and polishable.

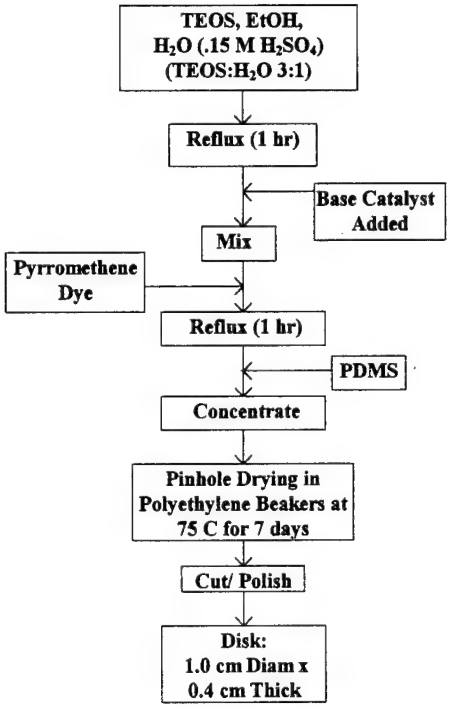

Figure 1: Synthetic Route for a PM-567 SiO_2:PDMS Polyceram.

Absorption Photostability. Samples were exposed to a long wave UV lamp (>300 nm, 8 Watts) at a distance of 1.5 inches . The absorption spectra of the samples were monitored periodically with a UV-VIS spectrophotometer (Perkin-Elmer,

Lambda 3B). The maximum absorption of the dye was normalized to the absorption before UV exposure and plotted as a function of UV exposure time. The permanent drop in the absorption represents the degradation of the dye.

Fluorescence Photostability. Photostability was also measured by monitoring the fluorescence intensity as a function of the number of pump pulses from a Q-switched, frequency doubled Nd:YAG laser (Quanta-Ray DCR-11) at 532 nm with a pulse rate of 10 Hz, a pulse width of 6 nsec, a pulse energy of 28 mJ, and a spot size of 0.6 cm in diameter. The samples were pumped while placed within a 6 inch integrating sphere. The exiting light was passed through color filters and a spectrometer in order to collect only the fluorescent light from the sample. The spectrometer was adjusted to the wavelength which had the highest fluorescent intensity (near 577 nm). The intensity of the light exiting the spectrometer was monitored by a silicon detector. A schematic of the photostability setup is shown in Figure 2[9].

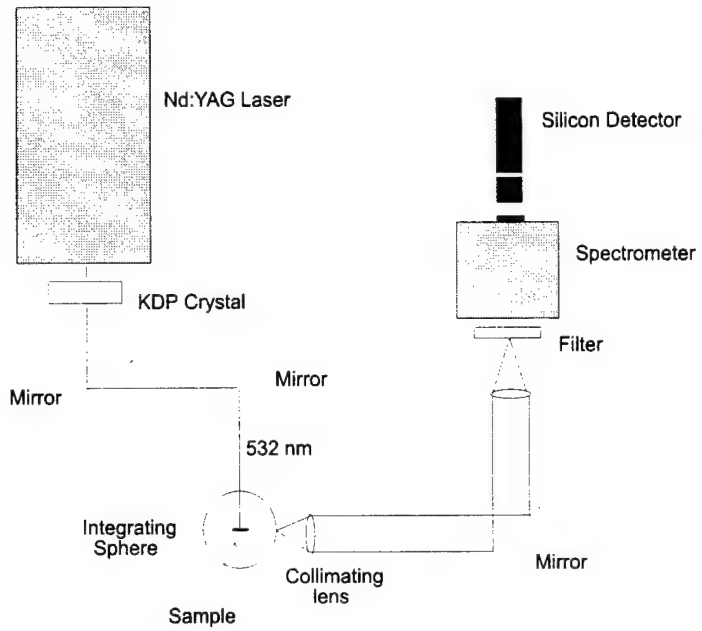

Figure 2: Schematic of the photostability measurement setup.

3. MECHANISM OF DEGRADATION

To improve the photostability of a particular dye/host system, one must first understand the mechanism(s) by which the dye degrades. An organic dye in its excited state can return to ground state by a number of pathways as shown in Figure 3. A number of these pathways are photochemical in nature such as dissociation, substitution, oxidation, hydrogen abstraction, and addition reactions[10-12]. These photochemical processes result in permanent destruction of the dye molecule. Hence in order to improve photostability, one must prevent or hinder these photochemical processes.

Review of the literature reveals that many laser dyes degrade by oxidation. This mechanism of decay was tested for the PM-567 in Polyceram monoliths. Three identical PM-567 SiO_2:PDMS Polycerams (dye concentration = $5*10^{-5}$ M, sample thickness = 0.15 cm) were placed in sealed fused silica cuvettes, and an over pressure of compressed air, oxygen, or argon was passed through the cuvettes while the samples were exposed to UV light (>300 nm). The absorption photostability is shown in Figure 4. The presence of oxygen caused a dramatic decrease in the photostability. In an oxygen atmosphere >90% of the dye degraded after 74 hours; while in an argon atmosphere, only 16 % of the dye degraded in the same period. In air, the rate of photodegradation was similar to that in an oxygen atmosphere. These results suggest that oxygen plays a role in the degradation of the dye.

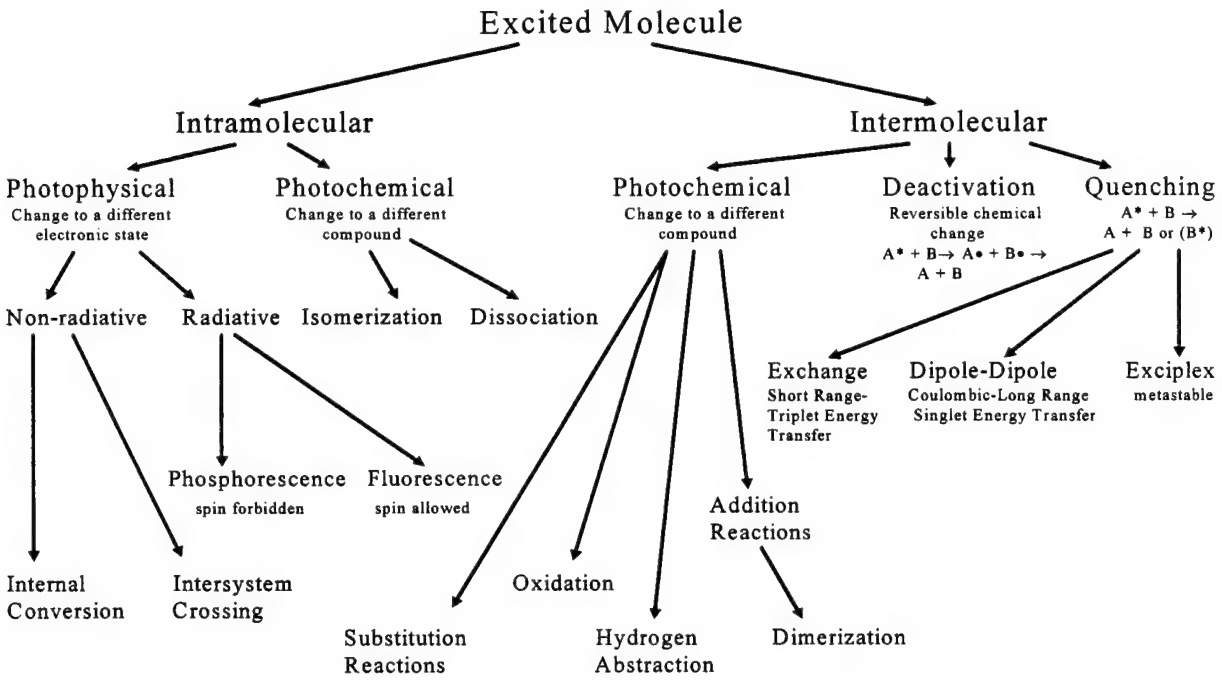

Figure 3: Decay pathways for an excited dye molecule.

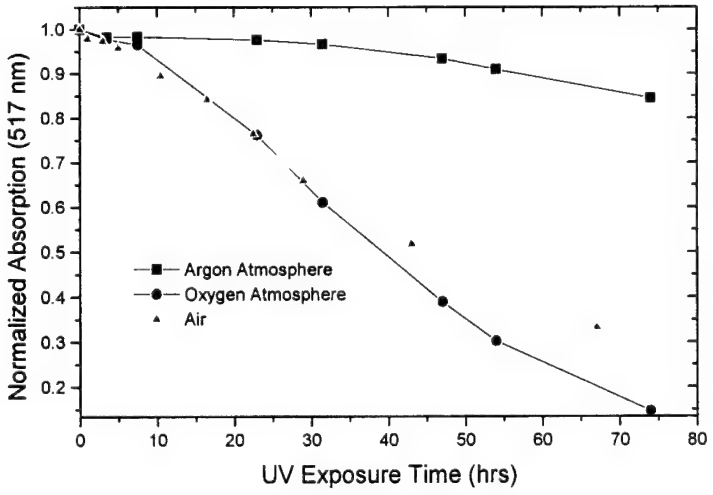

Figure 4: Absorption photostability of PM-567 doped SiO_2:PDMS Polycerams in different atmospheres.

The degradation products of PM-567 were then determined by chemical analysis to confirm that oxidative products were formed. Performing chemical analysis of photo-degradation products is often difficult because the dye is dissolved in hosts at fairly low concentrations of 10^{-3} to 10^{-5} M, resulting in very small yields of degradation products. To maximize the yield of degradation product, a custom quartz sealed cell was designed and constructed, offering a short path length (0.3 cm), a large surface area (10 cm x 10 cm) for UV lamp excitation, and a relatively large sample volume (30 ml compared to a conventional quartz cell with 3 ml). PM-567 was dissolved in ethanol (EtOH) at a concentration of $4*10^{-3}$ M, and a high

intensity UV Lamp (365 nm, 7000 $\mu W/cm^2$) was used to degrade the PM-567/EtOH solution for 48 hours. Before degradation, the solution was opaque red in white light; after degradation, the solution was transparent yellow. The product was isolated by evaporating the solvent. Using ^{13}C NMR spectroscopy, a single major product was determined, 3-ethyl-2-methylmaleimide (-8.4 ppm, -12.6 ppm, -17.0 ppm, -137.6 ppm, -143.3 ppm, -171.96 ppm, -172.3 ppm). The presence of the C=O groups in this product (Figure 5 (d)) confirms that the degradation occurs by oxidation. Alkyl pyrroles (Figure 5 (c)) are known to oxidize to form maleimide compounds[13-15]. Hence it is proposed that an alkylpyrrole is an intermediate product in the degradation of the dye. The degradation products were found to vary in composition upon change in acid or basic environment, but always contained C=O substituents verifying that the dye still degraded by oxidation.

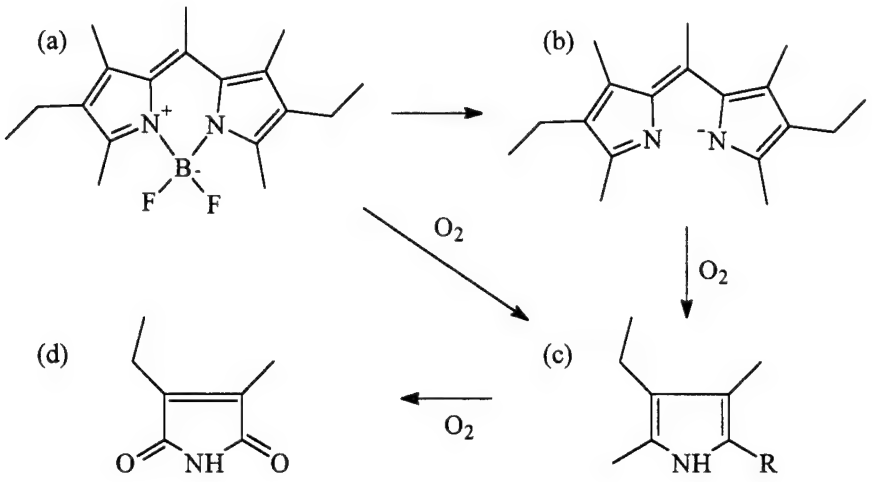

Figure 5: Proposed degradation route for (a) PM-567 by oxidation to (d) 3-ethyl-2-methylmaleimide.

The PM-567 dye was also found to degrade by chemical means. The chemical stability of PM-567 in the Polyceram solutions depended strongly on the catalyst(s) used to promote the sol-gel hydrolysis and condensation reactions. Reactions carried out with a highly acidic catalyst (e.g., HCl, H_2SO_4) resulted in complete bleaching (or degradation) of the dye molecules during sol-gel synthesis. Weaker acids used as catalysts (e.g., p-toluenesulfonic acid, HNO_3), also resulted in significant dye degradation, indicated by a large drop in dye absorptivity and a blue shift in the spectrum of the dye. Such processing conditions resulted in little or no visible fluorescence from the solutions upon UV lamp excitation (Table 1).

Table 1: Effect of catalyst on optical properties of the Polyceram solutions.

Catalyst used	pK_a	Solution Color	Absorption Maximum (nm)	Absorption at 517 nm	Fluorescence
HCl	-7.0	colorless	none	0.00	no
p-toluene sulfonic acid	-6.0	red/ brown	498	0.50	no
HNO_3	-1.4	red/ orange	501	0.40	minimal
HCl /pyridine	5.25	orange	369, 516	1.90	yes
HCl / triethylamine	11.0	orange	372, 517	0.97	yes

To ensure the stability of the PM dye and to maintain the high optical quality of the sol-gel host, hydrolysis was first carried out under acidic conditions (pH=2.2), and a base (e.g., pyridine, triethylamine) was added to neutralize partially the solution (final pH=5-6) before the addition of PM-567. This procedure allowed for safe incorporation of PM-567 within the Polyceram host. The effect of different catalysts used during the chemical synthesis of the Polyceram solutions on the absorption properties are summarized in Table 1. Dye degradation is reduced or prevented by neutralization of the solution.

The pyrromethene-BF_2 complex bond is likely the weakest link in the structure of PM-567. During synthesis of the dye, BF_3 was added to 2,6-diethyl-1,3,5,7,8-pentamethylpyrromethene hydrochloride salt under basic conditions to form the pyrromethene-BF_2 complex. When the dye is exposed to acidic environments, the complex bond will break. Knowing that PM-567 degrades by both photo-oxidation and by acidic degradation, a possible multi-step degradation process has been proposed [8]: (1) acidic removal of the BF_2, (2) oxidation of the C=C located between the cyclic rings, and (3) oxidation of the resulting alkylpyrroles to form maleimides (Figure 5).

Since O_2 plays a strong role in the degradation of the dye, it is useful to discuss the implications of the presence of O_2 in solvent and solid hosts. The concentration and diffusivity of O_2 in different hosts is summarized in Table 2. Comparing the O_2 concentration in air to that in solvent and PDMS, it is clear that a large amount of O_2 is present in the host. In fact, the dye concentration of PM-567 in a PDMS host is $6*10^{17}$ cm^{-3} ($5*10^{-5}$ M), while the concentration of O_2 in PDMS is $4.7*10^{18}$ cm^{-3}. The concentration of O_2 exceeds the dye concentration by a factor of 8. Clearly, at low dye concentrations there is more than enough O_2 already present in the host to oxidize all the dye.

Table 2: Solubility and diffusivity of O_2 in various hosts.

Host	Solubility or concentration of O_2	Diffusivity of O_2
Air (or pores in solid host)	$6*10^{18}$ cm^{-3}	10^{-1} cm^2/sec
Solvent	$1.2*10^{18}$ cm^{-3} ($2*10^{-3}$ M)[16]	$\approx 10^{-4}$-10^{-5} cm^2/sec
PDMS	$4.7*10^{18}$ cm^{-3} [17]	$1.7*10^{-5}$ cm^2/sec [17-19]
SiO_2 glass	----	$\approx 10^{-18}$ cm^2/sec[20] 10^{-23} cm^2/sec[21]

The diffusivity of O_2 decreases by orders of magnitude from air to solvent to PDMS (Table 4.3). However, the diffusivity of O_2 in PDMS compared to that in most solid polymers is very high, $1.7*10^{-5}$ cm^2/sec. Most glassy polymers have O_2 diffusion coefficients around 10^{-6}-10^{-7} cm^2/sec, while crystalline polymers have values of 10^{-7}-10^{-10} cm^2/sec[18, 19]. In fused silica glass, the diffusion of O_2 is close to zero at room temperature. Hence a dye molecule surrounded by a silica cage should be protected from O_2. No data could be found for the diffusion of O_2 through a SiO_2 xerogel; but it is presumed that the O_2 diffusion is governed by the amount of porosity present since O_2 diffusion through the pores is rapid.

Within a SiO_2:PDMS Polyceram, the diffusion of O_2 will depend on many factors including the polymer content and the porosity of the host. At low polymer contents, the SiO_2 matrix is continuous, and the O_2 diffusion will depend on the porosity of the sample. When interconnected porosity is present, the diffusion of O_2 through the bulk material should approach that in air (10^{-1} cm^2/sec), while with no interconnected porosity or regions of polymer, the diffusion of O_2 should be very low. At high polymer contents, the PDMS is continuous, and the diffusivity should be close to that of O_2 in PDMS. The Polyceram monoliths typically had a thickness of 0.4 cm. Using the diffusivity of O_2 in PDMS, the time required for O_2 to diffuse half way into the sample (0.2 cm) is about 40 min. Hence synthesizing the Polycerams under oxygen-free conditions would be useful, only if the material were used in oxygen-free environments or were provided with a O_2-barrier coating.

4. MOLECULAR ENGINEERING

4.1 Covalently attaching Laser Dye to Host

Silylated dyes (also referred to as grafted or functionalized dyes) are dye molecules which have been chemically altered to provide alkoxysilane functionality. This allows the dye molecule itself to participate in the hydrolysis and condensation reactions during sol-gel processing. The result is a covalently bonded active molecule within a host.

Numerous silylated Coumarin dyes have been synthesized by our group with varying degrees of functionality and linkages. These dyes have been incorporated within SiO_2 xerogel hosts and their optical properties (absorption and fluorescence spectra, fluorescence efficiency and photostability) have been characterized in detail elsewhere [7, 22-24]. The use of a silylated laser

dye resulted in: (1) improved solubility of the silylated dye with respect to its unsilylated counterpart, allowing for higher concentration of active molecules within a sol-gel matrix; (2) higher fluorescence efficiency, attributed to the greater rigidity and isolation of the silylated dye within its host; (3) improved chemical stability, associated with the lack of leachability of the dye from the host; (4) control of dye/matrix interactions affecting optical spectra; and most importantly, (5) improved photostability. The improved photostability is attributed to the greater probability of trapping the silylated dye in a closed silica cage, protecting it from impurities such as O_2. The proposed structures for a conventional and a covalently bound Coumarin 4 (7-hydroxy-4-methylcoumarin) dye in a SiO_2 xerogel host are shown in Figure 6, illustrating the differences in the degree of caging.

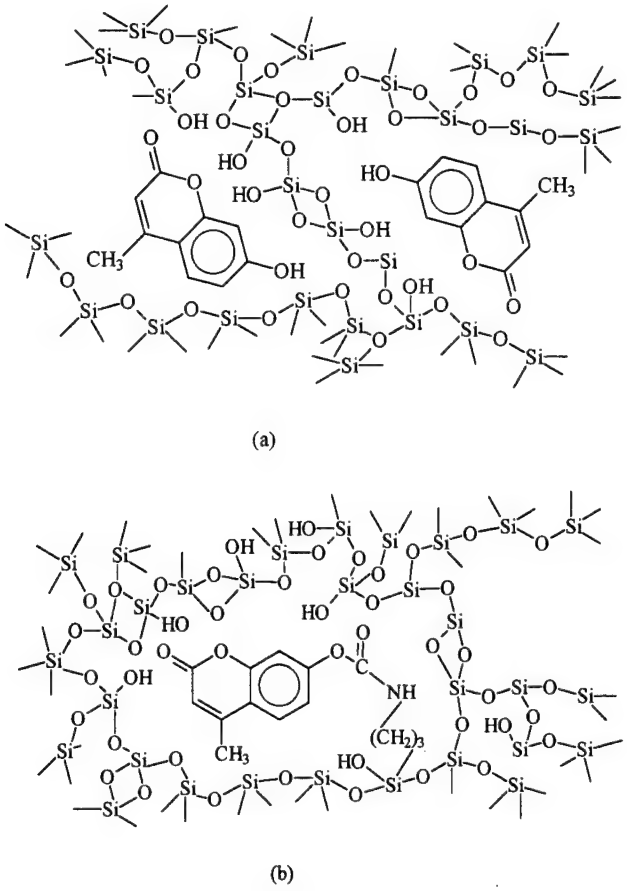

Figure 6: Proposed Structure of a (a) conventional Coumarin 4 laser dye (b) covalently bound Coumarin dye within a SiO_2 xerogel.

4.2 Porosity and host composition

The porosity and host composition were found to affect greatly the photostability of PM-567 within Polyceram hosts. Through variations of processing conditions (water content, reflux times, drying conditions) and composition (PDMS content), it was possible to control the porosity. Details of the processing are described elsewhere[8]. The 20% PDMS Polyceram (a Polyceram whose composition is 20 volume % PDMS and 80 vol % SiO_2) had a surface area of 740 m^2/gm (pore volume=63%); the 40% PDMS Polyceram had a surface area of 500 m^2/gm (pore volume=37%); the 60% PDMS Polyceram was essentially nonporous. The absorption photostability of these samples reveals that as the polymer content increases, the photostability improves (Figure 7a). The improvement in the photostability is attributed to the reduction in pore volume The dye molecules which are located within the pores are more susceptible to dye degradation, since O_2 has easier access to the dye molecules in the pores than to dyes located in polymer or silica cages. Also, dyes located within the pores

have more rotational, vibrational, and translational modes of excitation, and are therefore more susceptible to degradation and quenching.

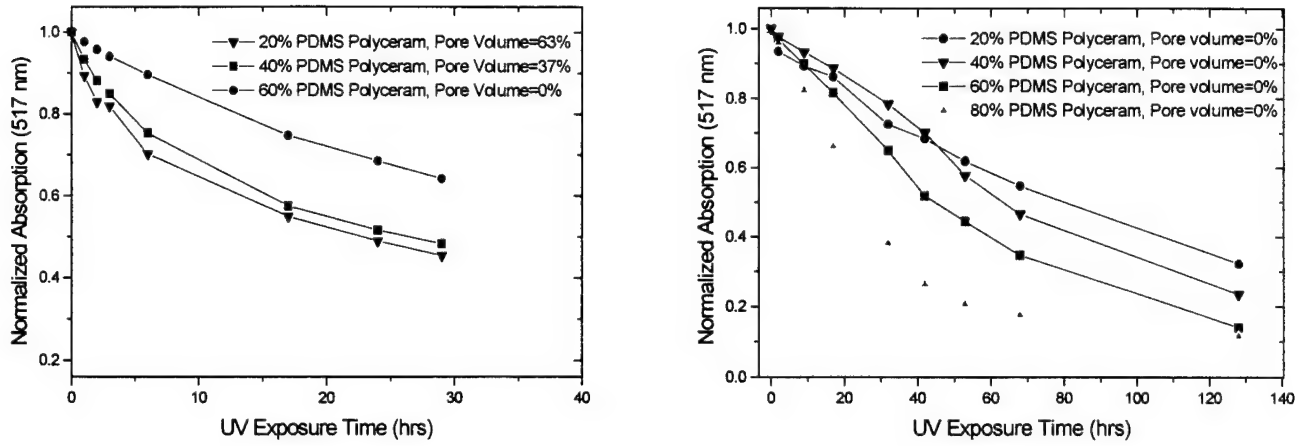

Figure 7: (a) Absorption photostability as function of PDMS content for PM-567 Polycerams synthesized by a route in which the porosity was a function of the PDMS content (b) Absorption photostability as function of PDMS content for PM-567 Polycerams synthesized by a route in which all compositions were nonporous.

By using another processing route (utilizing lower water content, shorter reflux times, and faster drying), it was possible to obtain nonporous samples for all PDMS contents. The absorption photostability of the nonporous Polycerams is shown in Figure 7b. The photostability improved with increasing silica content (reduction in PDMS content). Since all these samples were nonporous, it seems that a silica caging environment is required to improve further the photostability. The SiO_2-rich regions increase with decreasing PDMS content of the Polycerams.

The fluorescence photostability (shown in Figure 8) of these materials provides further evidence that porosity within the host leads reduced photostability. The nonporous Polyceram maintained more than 60% of its output after 50,000 pulses, while the fluorescence intensity of the porous sample of the same composition dropped to 60% after only 10,000 pulses. The porosity within the host tends to affect the initial drop in fluorescence more than the long term decay in the fluorescence. Several other groups have observed this initial drop in fluorescence[25-28]. The results in Figure 8 are likely associated with the heterogeneity of the photostabilities of the dye molecules within the host. The dye molecules are located within a variety of environments within the matrix, ranging from dyes located in open pores, to molecules in PDMS cages, to molecules in hybrid PDMS-SiO_2 cages, to molecules in SiO_2 cages[8]. Dye molecules located in the open pores of the host degrade first, and dye molecules located in SiO_2 cages take much longer to degrade.

The photostability of a sample depends not only on the laser dye and the host composition and structure, but also on factors such as the dye concentration, pump wavelength, pulse rate[29, 30], pump fluence[31], sample thickness[29], and geometry. With all these parameters, it is difficult to compare photostability measurements performed by different research groups. Several groups have used a parameter in GJ/mole representing the accumulated pump energy absorbed by the system per mole of dye molecules before the output pulse energy drops to half its initial value[32]. For the pump conditions explored here, the normalized photostability is 276 GJ/mole for the nonporous Polyceram and 87 GJ/mole for the porous Polyceram.

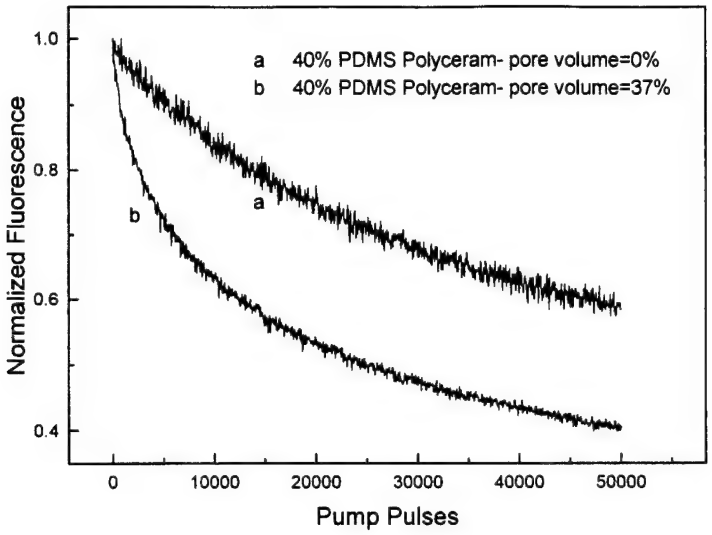

Figure 8: Effect of sample porosity on the fluorescence photostability of PM-567 in SiO_2:PDMS Polycerams containing 40% PDMS.

4.3 Additives to improve photostability

Additives to the host composition can be used to prevent photo-oxidation of the dye and to provide a more stable chemical (acid/base) environment, resulting in improved photo/chemical stability. Antioxidants are molecular species which interfere with the oxidation process by a variety of mechanisms. There are many types of antioxidants, and choosing the proper antioxidant depends on the host composition, the application, the solubility of the antioxidant in the host, the volatility of the antioxidant, and the mechanism of oxidation. Most antioxidants are used in the food industry and for polymer stabilization. In this study, antioxidants are used for dye stabilization. Antioxidants can be divided into five major classes, listed below with their effect on dye stability[33]:

1) **Absorber:** A molecule which preferentially absorbs photons which would normally be absorbed by the dye.
2) **Deactivator:** A molecule or metal complex which quenches the dye in its excited state.
3) **Interceptor:** A molecule which slows oxidation by preferentially reacting with O_2 or by quenching excited state O_2 (singlet O_2).
4) **Free radical scavenger (Primary antioxidant):** A molecule which preferentially reacts with free radicals such as alkyl radicals ($R^{\bullet}$) and peroxy radicals ($R\text{-}O\text{-}O^{\bullet}$).
5) **Decomposer (Secondary antioxidant):** A molecule which reacts with hydroperoxides to prevent the formation of free radicals which accelerate dye degradation.

For laser dyes, absorbers and deactivators are not good choices since they will affect the ability of the dye to fluoresce. Hence interceptors and free radical scavengers are utilized in the present study.

Three additives were chosen. The first two are free radical scavengers, Tinuvin 770 and 2,2,6,6-tetramethylpiperidine (TMP), which are also known as hindered amine light stabilizers (HALS). The hindered amine groups (>NH) in these antioxidants are oxidized to form nitroxyl radicals ($>NO^{\bullet}$) which preferentially react with free radicals of the dye molecule[34-36]. This prevents the dye radicals from initiating further reactions. The third additive, 1,4-diazobicyclo[2.2.2]octane (DABCO), is a known singlet O_2 quencher and has been used in the past for improving the photostability of laser dyes[37, 38]. DABCO is an interceptor, which works by quenching singlet O_2 thus preventing excited-state O_2 from reacting with the dye molecules. The structure and properties of the additives discussed above are shown in Table 3.

Table 3: Properties of antioxidant and base additives.

Additive	Type	Structure	Properties
(Tinuvin 770) bis(2,2,6,6-tetramethyl-4-piperidinyl) sebacate	HALS	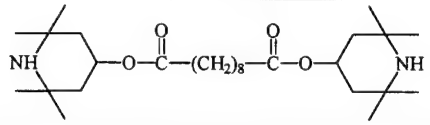	mw 481 mp 83 C
(TMP) 2,2,6,6 tetramethylpiperidine	HALS	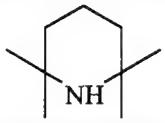	mw 141.26 bp 152C fp 24C
(DABCO) 1,4-diazobicyclo[2.2.2] octane or triethylene diamine	Singlet oxygen quencher		mw 112.18 mp 159C fp 94C pKa 8.8

mw= molecular weight, mp= melting point, fp= flash point

The absorption photostability of PM-567 in EtOH at 10^{-5} M plus 1 wt % of each additive are shown in Figure 9. All the additives showed improved photostability with respect to the control (PM-567 in EtOH with no additive); the largest improvement was observed with the Tinuvin 770 additive. Since all the additives here are bases, the improvement in photostability could be attributed solely to the basic characteristic of the additive. However, this is not likely since the addition of DABCO, a strong base (pKa=8.8), resulted in a lower photostability than the addition of Tinuvin 770, a weaker secondary amine base (pKa=10.8-11.0). The results of this study suggest that antioxidant additives can be effective in improving the photostability of dye/host systems. Work is currently in progress in our group to incorporate these additives within dye doped Polyceram hosts.

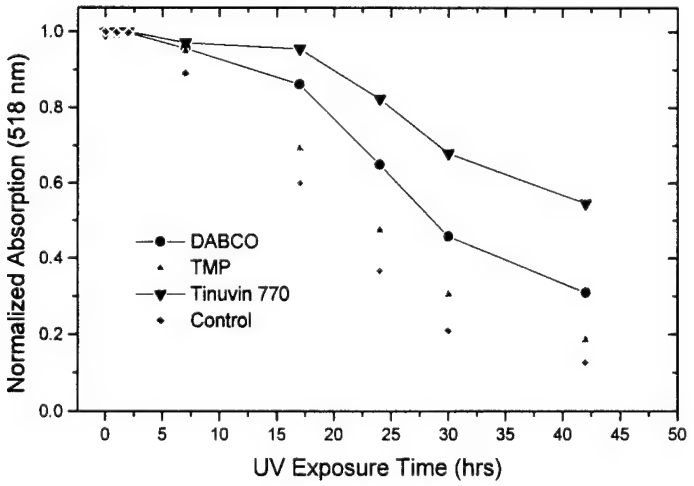

Figure 9: Absorption photostability of PM-567 in EtOH at 10^{-5} M with various additives at 1 wt %.

CONCLUSIONS

Molecular engineering techniques to control the dye/host interactions have been proven to be effective for improving the photostability of laser dyes within sol-gel derived hosts. The degradation of PM-567 was determined to occur by photo-oxidation and by acid environments. Improved photostability was observed under the following conditions: when irradiation was carried out in an oxygen-free atmosphere; when the dye was covalently bound to the host; when porosity was removed from host; when the dye was highly caged within the SiO_2 environment; when the dye was placed a chemically compatible environment; and when certain additives were added to the hosts. These molecular engineering techniques can be used for designing and synthesizing highly photostable dye/host systems.

ACKNOWLEDGEMENTS

The financial support of the Air Force Office of Scientific Research, the Corning Foundation Fellowship, and the Chapman Fellowship are gratefully acknowledged.

REFERENCES

1. R. O'Connell, T. Saito, "Plastics for High-Power Laser Applications: A Review," *Optical Engineering* 22, 393-399 (1983).
2. R. Fitzpatrick, "Laser in Dermatology & Plastic Surgery," *Optics & Photonics News* 6, 23-31 (1995).
3. H. Aldag, "Solid-State Dye Laser For Medical Applications," *Visible and UV Lasers* SPIE 2115, 184-189 (1994).
4. M. Hamblin, T. Hasan, "Advances in Photodynamic Theory," *Optics & Photonics News* 7, 16-21 (1996).
5. J. Manni, "High Powered Delivery: Fiberoptic Laser Surgery," *Optics & Photonics News* 7, 23-28 (1996).
6. B. Ropoulos, "Medical Lasers," *Photonics Spectra* June, 116-120 (1996).
7. T. Suratwala, Z. Gardlund, K. Davidson, D. R. Uhlmann, J. Watson, N. Peyghambarian, "Silylated Coumarin Dyes in Sol-Gel Hosts. I. Structure and Environmental Factors on Fluorescent Properties," *Chemistry of Materials* , to be submitted (1997).
8. T. Suratwala, "Photostability of Laser Dyes in Sol-Gel Derived Hosts", Ph.D. Thesis, University of Arizona (1996).
9. T. Suratwala, Z. Gardlund, K. Davidson, D. R. Uhlmann, S. Bonilla, N. Peyghambarian, "Processing and Photostability of Pyrromethene 567 in Polyceram Monoliths," *Journal of Sol-Gel Science and Technology* , to be published (1996).
10. M. Klessinger, J. Michl, *Excited States and Photochemistry of Organic Molecules* (VCH Publishers, Inc., New York, 1995).
11. J. Coyle, *Introduction to Organic Photochemistry* (John Wiley & Sons, Chichester, 1986).
12. W. Horspool, P. Song, Eds., *CRC Handbook of Organic Photochemistry and Photobiology* (CRC Press, Boca Raton, 1995).
13. G. Gardini, "The Oxidation of Monocyclic Pyrroles," *Advances in Heterocyclic Chemistry* 15, 67-99 (1973).
14. M. George, V. Bhat, "Photooxygenation of Nitrogen Heterocycles," *Chemical Reviews* 79, 447-478 (1979).
15. G. Quistad, D. Lightner, "Pyrrole Photo-Oxidation. The Direct Formation of Maleimides," *Chemical Communications*, 1099-1100 (1971).
16. A. Frimer, *Singlet O_2* (CRC PRESS, Boca Raton, 1985), vol. I.
17. B. Arkles, "Gelest: Metal Organics Including Silanes and Silicones," *Product Catalog* (1995).
18. S. Pauly, "Permeability and Diffusion Data," in *Polymer Handbook* J. Brandrup, E. Immergut, Eds. (John Wiley & Sons, New York, 1989), vol. VI, pp. 435-449.
19. V. Stannett, "Simple Gases," in *Diffusion in Polymers* J. Crank, G. Park, Eds. (Academic Press, London, 1968) pp. 40-73.
20. W. Kingery, H. Bowen, D. R. Uhlmann, *Introduction to Ceramics Second Edition* (John Wiley & Sons, New York, 1976).
21. J. Schaffer, A. Saxena, S. Antolovich, T. Sanders, S. Warner, *The Science and Design of Engineering Materials* (Irwin, Chicago, 1996).
22. F. Schafer, *Dye Lasers* (Springer-Verlag, New York, 1973).
23. T. Suratwala, Z. Gardlund, J. M. Boulton, D. R. Uhlmann, J. Watson, N. Peyghambarian, "Incorporation of Triethoxysilyl Functionalized Coumarin 4 in Sol-Gel Hosts," *Sol-Gel Optics III* SPIE 2288, 310-320 (1994).
24. T. Suratwala, Z. Gardlund, K. Davidson, D. R. Uhlmann, S. Bonilla, N. Peyghambarian, "Processing and Photostability of Silylated Coumarin Dyes in Polyceram Hosts," *Journal of Sol-Gel Science and Technology* , to be published (1996).

25. G. He, J. Bhawalker, C. Zhao, P. Prasad, "Properties of Two-Photon Pumped Cavity Lasing in Novel Dye Doped Solid Matrices," *IEEE Journal of Quantum Electronics* 32, 749-755 (1996).
26. J. McKiernan, S. Yamanaka, B. Dunn, J. Zink, "Spectroscopy and Laser Action of Rhodamine 6G Doped Aluminosilicate Xerogels," *J. Phys. Chem.* 94, 5652-5654 (1990).
27. R. Sastre, A. Costela, "Polymeric Solid-State Dye Lasers," *Advanced Materials* 7, 198-202 (1995).
28. Y. Kobayashi, Y. Imai, Y. Kurokawa, "Preparation of a Transparent Alumina Film Doped with Organic Dye by the Sol-Gel Process," *Journal of Material Science Letters* 7, 1148-1150 (1988).
29. M. Canva, P. George, J. Perelgritz, A. Brum, F. Chaput, J. Boilot, "Perylene- and Pyrromethene-doped Xerogel for a Pulsed Laser," *Applied Optics* 34, 428-431 (1995).
30. M. Canva, A. Dubois, P. Georges, A. Brun, F. Chaput, A. Ranger, J. Boilot, "Perylene, Pyrromethene, and Grafted Rhodamine Doped Xerogels for Tunable Solid State Laser," *Sol-Gel Optics III* SPIE 2288, 298-309 (1994).
31. B. Dunn, F. Nishida, R. Toda, J. Zink, T. Allik, S. Chandra, J. Hutchingson, "Advances in Dye-Doped Sol-Gel Lasers," *Mat. Res. Soc. Symp. Proc.* 329, 267-277 (1994).
32. M. Rahn, T. King, "Comparison of Laser Performance of Dye Molecules in Sol-Gel, Polycom, Ormosil, and Poly(methyl methacrylate) Host Media," *Applied Optics* 34, 8260-8271 (1995).
33. A. Frimer, *Singlet O_2* (CRC Press, Boca Raton, 1985), vol. IV.
34. N. Allen, J. Kotecha, "Thermal Antioxidant Properties of Hindered Piperidine Light Stabilizers and Further Studies on Photo-Chemical Oxidation," *Polymer Degradation and Stability* 11, 181-194 (1985).
35. T. Kurumada, H. Ohsawa, O. Oda, T. Fujita, T. Toda, T. Yoshioka, "Photostabilizing Activity of Tertiary Hindered Amines," *Journal of Polymer Science* 23, 1477-1491 (1985).
36. J. Sedlar, J. Petruj, J. Pac, M. Navratil, "Polymer Polymerization by HALS derivative: the role of piperidine-hydroperoxide association," *Polymer* 21, 5-7 (1980).
37. K. Priyadarsini, "Effect of 1,4-diazabicyclo-[2,2,2]-octane on the laser properties of 7-amino coumarin dyes," *J. Photochem. Photobiol. A: Chem* 61, 381-388 (1991).
38. F. Schafer, "Dye Lasers and Laser Dyes in Physical Chemistry," in *Dye Laser: 25 Years* M. Stuke, Ed. (Springer-Verlag, Berlin, 1992), vol. 70, pp. 19-36.

Keywords: water soluble silica, colloids, 3-aminopropyltriethoxysilane, tetramethoxysilane, reversible gel, DLVO theory

To contact author:
Dr. Tayyab Suratwala
University of California
Lawrence Livermore National Laboratory
7000 East Avenue L-487
Livermore, CA 94550

(510) 422-1884 (office)
(510) 422-1210 (Fax)
Suratwala1@llnl.gov

Control of Porosity in SiO_2:PDMS Polycerams through Variations in Sol-Gel Processing and Polymer Content

T. Suratwala, K. Davidson, Z. Gardlund, and D.R. Uhlmann
Department of Materials Science and Engineering, Arizona Materials Laboratory
University of Arizona, 4715 E. Fort Lowell, Tucson, AZ 85712, USA

ABSTRACT

A series of optically transparent SiO_2: polydimethylsiloxane (PDMS) Polyceram monoliths have been synthesized by two-step acid/base sol-gel processes. Two different processing routes are discussed and compared; one synthetic route (Route 1) utilizes lower water content, shorter reflux times, and faster drying conditions compared to the other synthetic route (Route 2). The Route 1 Polycerams were all essentially non-porous at all PDMS contents examined (20-80 volume % PDMS). In contrast, the porosity of the Route 2 Polycerams varied dramatically as a function of PDMS content. The surface area and pore volume for a 0% PDMS Route 2 Polyceram were 573 m^2/gm and 0.59 cm^3/gm, respectively; the surface area and pore volume decreased with increasing PDMS content. The amount of porosity within the Polycerams is proposed to be controlled by the relative rates of condensation and evaporation during processing and by the amount of PDMS trapped in the pores. This ideas supported by the differences in the drying behavior with processing and by the structural information obtained by magic angle spinning solid-state ^{29}Si NMR of the Polyceram monoliths. Quantitative evaluation of the ^{29}Si NMR and porosity data are utilized to formulate structural models of these Polycerams. The structural models are then specifically used to describe the effect of porosity on the photostabilization of a laser dye doped within these Polyceram monoliths.

KEYWORDS: Porosity, Polydimethylsiloxane, Polycerams, Surface Area, MAS ^{29}Si NMR, N_2 adsorption BET, Pyrromethene 567, photostability

1. INTRODUCTION

Engineered porous materials are useful for a variety of important technologies including filters, absorbers, separation systems for gases, ions, small molecules and particles, low dielectric substrates, and thermal insulators[1]. Porous materials synthesized by sol-gel techniques represent an important class of engineered porous materials because of the ability to obtain a wide range of pore sizes and surface areas depending on the processing and composition. Sol-gel synthesized aerogels, xerogels, and porous vitrified silica have been extensively investigated for their porosities[2-5], while Polyceram materials, which are polymer-modified ceramic materials in which the organic and inorganic components are combined on a near-molecular scale, have only been recently studied[6-8].

A number of methods have been applied to control the porosity, surface area, and pore size distributions within sol-gel matrices. In a review by Brinker et. al.[3], these different techniques are discussed; a summary of these methods is illustrated in Table 1. One way to control the porosity is to manipulate the relative rates of condensation and solvent evaporation during sol-gel synthesis. When the condensation rate greatly exceeds the evaporation rate during drying, the material will tend to have a higher porosity. The high condensation rate increases the gel strength and limits the amount of shrinkage which takes place during drying. In contrast, when the evaporation rate exceeds the condensation rate, the material is more likely to shrink, resulting in a less porous material. A sol which is spin-coated to form a film is an example of the case where the evaporation rate is high with respect to the condensation rate. The condensation rate can be controlled by a number of factors such as the reactivity of the alkoxide, the pH of the solution, the catalyst, the nature and the amount of solvent present, and the H_2O:Si mole ratio. The evaporation rate can be controlled during drying by the solvent volatility, the drying temperature, the air flow, and the surface area of gel exposed to drying.

The effectiveness of varying the relative rates of condensation and evaporation for porosity control has been demonstrated with xerogels[3]; but to the authors' knowledge, this method has not been demonstrated with Polyceram materials. Non-porous materials have not been synthesized using this method with xerogels; only materials with decreased porosity have been achieved. With the incorporation of polymers or oligomers during synthesis, non-porous materials can be obtained. In the present study, we explore how porosity can be controlled within Polycerams by changes in the relative rates

of condensation and evaporation during processing. The porosity and surface area are related to the processing conditions and polymer content, and structural models are developed based on NMR and BET data. Finally, the control of porosity and the structural model are utilized to obtain insight into the effects of porosity on the photostability of a laser dye doped within these SiO_2:PDMS Polycerams.

Table 1: Methods explored to control porosity in sol-gel matrices.

Method	Principle of Method	Comments
Particle Packing	•packing of colloidal particles creates pores which have sizes related to particle size	•uniform pore size obtained with uniform particle size •pore volume for spherical particles is always 33% regardless of particle size, assuming dense random packing
Aggregation of Fractals	•pores form through the aggregation of polymeric sols	•works only if clusters don't interpenetrate or if there are no oligomeric species to "fill-in" pores
Management of Capillary Pressure	•vary capillary pressure (P_c) to achieve desired pore size during solvent removal •$P_c = -2\gamma/r$, where γ is the surface tension and r is the pore radius	•Methods •vary ambient pressure •vary surface chemistry (changes surface tension) •use drying control additives (DCCAs)[9, 10] •vary solvent composition •go to supercritical conditions
Molecular Templating	•pore size control by the size of solvent or organic ligand to be removed	•Example: pore size increases from methanol to ethanol to isopropanol solvent
Relative rates of condensation and evaporation	•porous when condensation rate >> evaporation rate •less porous or non-porous when evaporation rate >> condensation rate	•can control relative rates of condensation and evaporation through composition, processing, aging, and drying conditions
Sintering and Surface Derivitization	•sintering to higher temperatures reduces pore volume and pore size distribution •sintering occurs by the reduction of the solid vapor interfacial energy, which can be controlled by altering the surface of the gel	

2. EXPERIMENTAL

Material Synthesis. A low molecular weight (MW=400-700) silanol-terminated polydimethylsiloxane (PDMS) (United Chemical Technologies) was the reactive polymer used to make the Polycerams. The silanol end groups of the PDMS can participate in condensation reactions with a hydrolyzed metal alkoxide or another silanol-terminated PDMS. This can result in Metal-PDMS, or PDMS-PDMS linkages, respectively. Two synthetic routes were used, Route 1 and Route 2. All the resulting samples were optically transparent and polishable.

Route 1. Tetraethoxysilane (TEOS), PDMS, ethanol (EtOH), and H_2O (acidified to 0.15 M with H_2SO_4) were refluxed in a flask for 1 hour at a EtOH:H_2O:TEOS molar ratio of 35:2:1. PDMS was added at various concentrations ranging from 0% to 80% by volume with respect to the final solid volume. A base (triethylamine or 1,4-diazobicyclo[2.2.2]octane (Dabco)) was added at base:acid mole ratio of 2:1 and the solution was mixed for 15 minutes. Pyrromethene 567 (PM-567) laser dye (synthesis reported elsewhere[11, 12]) was then added at a concentration of $5*10^{-5}$ M and the solution was concentrated. Monoliths were made by pouring the solution in polypropylene beakers and drying at 75 C for 3 days. After polishing, the resulting Polyceram disks were 2 cm in diameter and 0.4 cm thick. This synthetic route is shown schematically in Figure 1a.

Route 2. TEOS, EtOH, and H_2O (acidified to 0.15 M with H_2SO_4) were refluxed in a flask for 1 hour at a EtOH:H_2O:TEOS molar ratio of 35:3:1. A base (triethylamine or Dabco) was added at base:acid mole ratio of 2:1 and the solution was mixed for 15 minutes. PM-567 was added at $5*10^{-5}$ M, the solution was refluxed for an additional hour, and then the PDMS was added. The solutions were then concentrated and dried in polyethylene beakers with pinhole tops at 75 C for one week. Samples were made at various PDMS contents in the solid Polyceram ranging from 0 % to 80 % by volume. This synthetic route is shown schematically in Figure 1b.

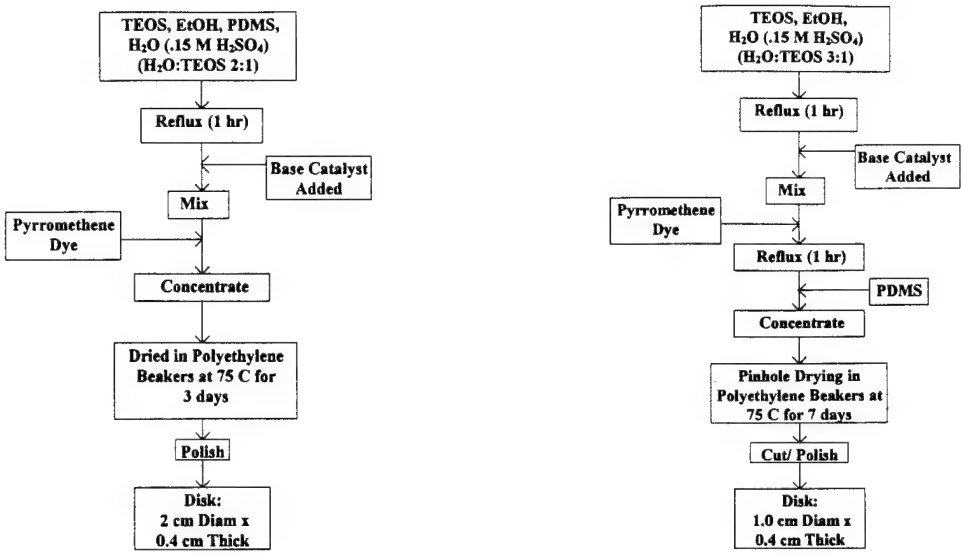

Figure 1: Schematic of SiO_2:PDMS Polyceram synthesized by (a) Route 1 and (b) Route 2.

Surface Area and Porosity Measurements. The surface area, pore volume, and pore size were determined by the N_2 (77 K) adsorption BET (Brunauer, Emmet, Teller) isotherm method[13] using a Micrometrics ASAP 2000 for the solid SiO_2:PDMS Polycerams. Typically, 0.5 gm of the solid Polyceram was degassed for 48 hours at 90 C in vacuum (10^{-6} Torr) before the adsorption measurements. All the porous samples showed Type I Isotherm behavior and fit well to the BET Isotherm. The effective cross sectional area of the N_2 cross section (which is needed to calculate the specific surface area of the material) is different for silica based materials compared with other materials[4, 14]. Ismail[14] measured silica samples with N_2 adsorption and Kr adsorption, and determined the effective cross sectional area of N_2 for silica to be 0.112 nm^2, instead of the more standard effective cross section 0.162 nm^2. The interaction of the quadrupole moment of the N_2 molecule with the hydroxyl groups on the silica surface is believed to cause the decrease in the effective cross section. The cross sectional area of N_2 determined by Ismail was used for all the porosity calculations reported here.

NMR Spectroscopy. Magic Angle Spinning (MAS) Cross Polarization (CP) ^{29}Si Nuclear Magnetic Resonance (NMR) was performed on the solid SiO_2:PDMS Polycerams using a Bruker Instruments model MSL-200. For the CP spectra, 5 ms contact time was applied, and for the MAS, a spinning rate of 3.5 kHz was used. Some samples were measured without CP in order to obtain more quantitative evaluation of the ratio of the Q species to be used in the structural model.

Density Measurements. The densities of the SiO_2:PDMS Polycerams were measured by placing the samples in a density gradient column. The gradient column was made using a 1:1 mixture of xylene (ρ=0.885 gm/cm^3) and carbon tetrachloride (ρ=1.58 gm/cm^3) within a 250 ml graduated cylinder [15]. The column was calibrated by placing polymeric pellets of known densities within the column, and the densities of the Polycerams were calculated based on the height at which the Polycerams settled in the gradient column.

3. RESULTS AND DISCUSSION

3.1 Control of Porosity as a Function of Processing

Using the BET method to evaluate the surface area and pore volume, the SiO_2:PDMS Polyceram monoliths with 40 % PDMS synthesized using Route 1 had no measurable porosity or surface area, while the monoliths with 40% PDMS synthesized by Route 2 had a high pore fraction (0.38) and a high surface area (342 m^2/gm). These results are explained in the discussion below.

Routes 1 and 2 (Figure 1) had specific differences in their processing, which lead to changes in the relative rates of hydrolysis and condensation. First, Route 2 utilized a higher water content (H_2O:TMOS mole ratio = 3:1) compared to Route

1 (H_2O:TMOS = 2:1). This resulted in a greater degree of condensation with the Route 2 Polycerams. Second, the Route 2 solutions were refluxed for an additional hour after the base catalyst was added, while the Route 1 solutions were not refluxed after the addition of the base. This resulted in a greater condensation rate with the Route 2 Polycerams. Third, the Route 2 solutions were pin-hole dried (i.e., dried in a covered polypropylene container with pin holes to allow evaporation), while the Route 1 solutions were open-top dried (i.e., dried in an uncovered polypropylene container). This resulted in a lower evaporation rate for Route 2 solutions, allowing more time for condensation to occur than with the Route 1 solutions.

These differences in the processing between Routes 1 and 2 lead to dramatic changes in the drying behavior of the Polyceram solutions (see Figure 2). A syneresis drying behavior, where the gel network contracts and expels the liquid from the pores[2], was observed with the Route 2 Polycerams. The syneresis behavior is attributed to condensation reactions forming new bonds and causing shrinkage of the gel, thus forcing the removal of solvent. The high degree of crosslinking resulted in a high gel strength; therefore, at some point during drying, the gel gained enough strength that it did not shrink any further. Hence further solvent removal resulted in the formation of external voids or porosity within the solid sample. The drying behavior for the Route 1 Polycerams was quite different (Figure 2). Large solvent removal preceded much of the condensation reactions, because the sample did not gel until most of the solvent was removed. Sample shrinkage was governed by the evaporation; hence these samples were essentially non-porous.

The use of acid/base two-step processes allowed control of the hydrolysis/condensation reactions (Figure 3a), because the reaction kinetics were greatly dependent on the pH of the solution. The general effect of pH on the gel time for aqueous silicates is summarized in Figure 3b[16]; similar pH behavior has been observed with the hydrolysis/condensation reactions of silicon alkoxides[2]. Under acidic conditions (pH=1-3), both the hydrolysis and condensation reactions are catalyzed, but the hydrolysis rate greatly exceeds the condensation rate. This results in weakly branched structures and relatively long gel times. Under less acidic conditions (pH=3-8), the condensation rate increases and the hydrolysis rate decreases, resulting in shorter gel times. The degree of hydrolysis and condensation can then be controlled by hydrolyzing under acidic conditions and then accelerating condensation reactions by adding a base. The amount of condensation which took place in the two-step acid/base processes employed here (Routes 1 & 2) was governed by the degree of hydrolysis in the first step. For example, under partial hydrolysis conditions, all the alkoxide groups were not hydrolyzed after the first step. Upon addition of the base, the condensation rate is enhanced. However, the water-producing condensation rate is greater than the alcohol producing condensation rate[2] (see Figure 3a). Hence the degree of condensation is largely limited to the number of hydrolyzed species.

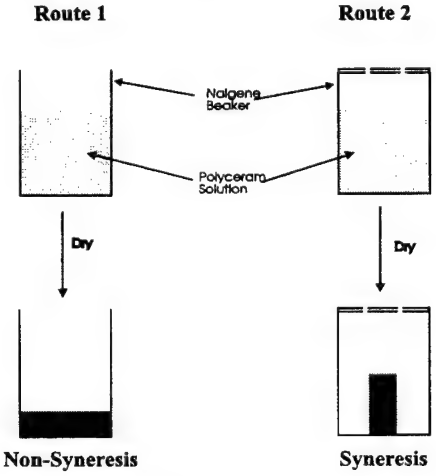

Figure 2: Differences in drying behavior of the SiO_2:PDMS Polyceram solutions processed using Routes 1 and 2.

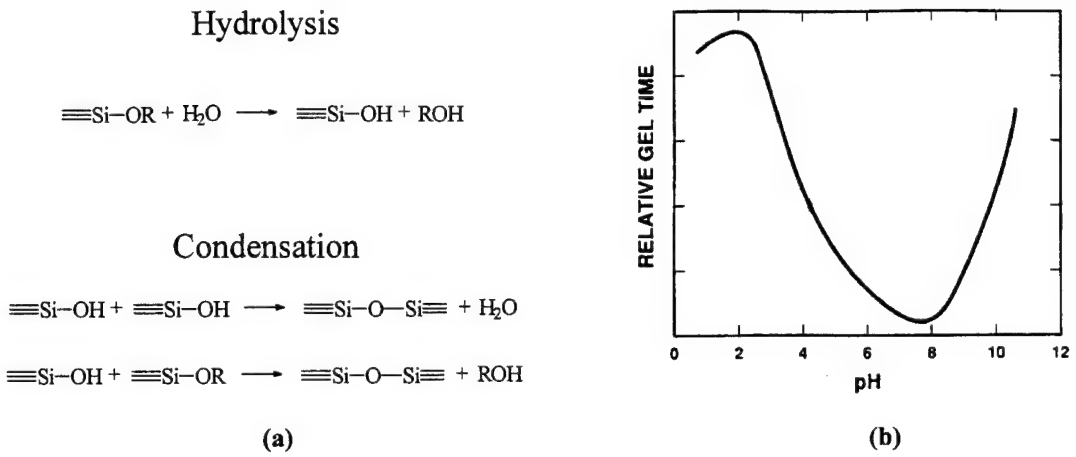

Figure 3: (a) Schematic of hydrolysis and condensation reactions and (b) gel time as a function of pH for aqueous silicates. After Iler[16].

Solid-state ^{29}Si NMR is a useful technique for examining the structure of silicates [17-21]. A variety of silicate structures can be formed in the sol-gel process and they can be described by three major silicate species: (1) Q species which represents a quartenary oxygen tetrahedron; (2) T species which represents a three oxygen, one alkyl group tetrahedron; and (3) D species which represents a two oxygen, two alkyl group tetrahedron. Superscripts after the Q, T, or D nomenclature denote the number of alkoxide groups which have reacted to form Si-O-Si linkages. Therefore, Q^0, T^0, and D^0 represent unreacted precursors, while Q^4, T^3, and D^2 represent completely reacted species. In this study, Q species signify Si-O species from TEOS, and D species signify Si-O species from PDMS. There are no T species in the present Polycerams. CP and MAS techniques were used to obtain enhanced signals and resolution with solid-state ^{29}Si NMR spectra. This technique was applied to determine the degree of silica and PDMS crosslinking within the Route 1 and Route 2 Polycerams. The CP-MAS ^{29}Si NMR spectra for all of the SiO_2:PDMS Polycerams used in this study are shown in Figure 4. Comparison of the NMR spectra for SiO_2:PDMS Polycerams.(40 volume % PDMS) synthesized by Routes 1 and 2 shows that the silica species are more crosslinked in the Route 2 Polyceram; the Route 2 Polyceram has less Q^1 and Q^2 species compared to the corresponding Route 1 Polyceram. This confirms the high degree of condensation of the Route 2 Polycerams with respect to the Route 1 Polycerams and supports our hypothesis of porosity control.

The interpretation of the crosslinking of the PDMS (D species) is more complex. D^2 and D^1 peak assignments have been previously reported with values of -19 to -23 and -12 ppm, respectively[17, 22, 23]. The PDMS oligomer contains approximately seven Si atoms. That means that five of the Si atoms have a D-D^2-D character, while the two Si atoms at the ends of the PDMS can have different types of bonding. In our system it is not possible to obtain the D^0 peak at -4.8 ppm[22, 23] because that could only occur if the monomer of PDMS was present in the system; only D^1 and D^2 peaks are possible. The amount of D^1 (-12 ppm) present was very small (<5%) in both 40% PDMS Polycerams (Figure 4), suggesting that most of the PDMS have condensed. A sharp D^2 peak at -23.5 ppm was observed with both samples, which represents both the Si atoms within the PDMS oligomer and the Si atoms connected to the silanol groups at the ends of the oligomer which have condensed to another PDMS (D-D^2-D).

Both samples also had an additional broad D^2 peak (referred to as D^{2*}) with chemical shifts between -18 to -21 ppm (Figure 4). The broad peak stems from the use of the CP technique, which enhances the intensity of Si atoms located near H atoms (<10 Å)[24]. The broad peak corresponds to D^{2*} units in more constrained environments. In other words, it represents D^2 species bonded to various Q species or D species trapped around a Q skeleton. This has been argued from the much longer CP relaxation time for the sharp D^2 peak (6.0 msec) compared to that of the broad D^{2*} peak (0.8 msec)[23]. In other silicate materials, CP relaxation times have been observed to decrease when the species are locally constrained. Broad D^{2*} peaks have also been identified with CP-MAS ^{29}Si NMR spectra of other PDMS/TEOS systems as well as in (dimethyldiethoxysilane) DEDMS / TEOS and DEDMS / (titanium tetraisopropoxide) TIP nanocomposites[23, 25].

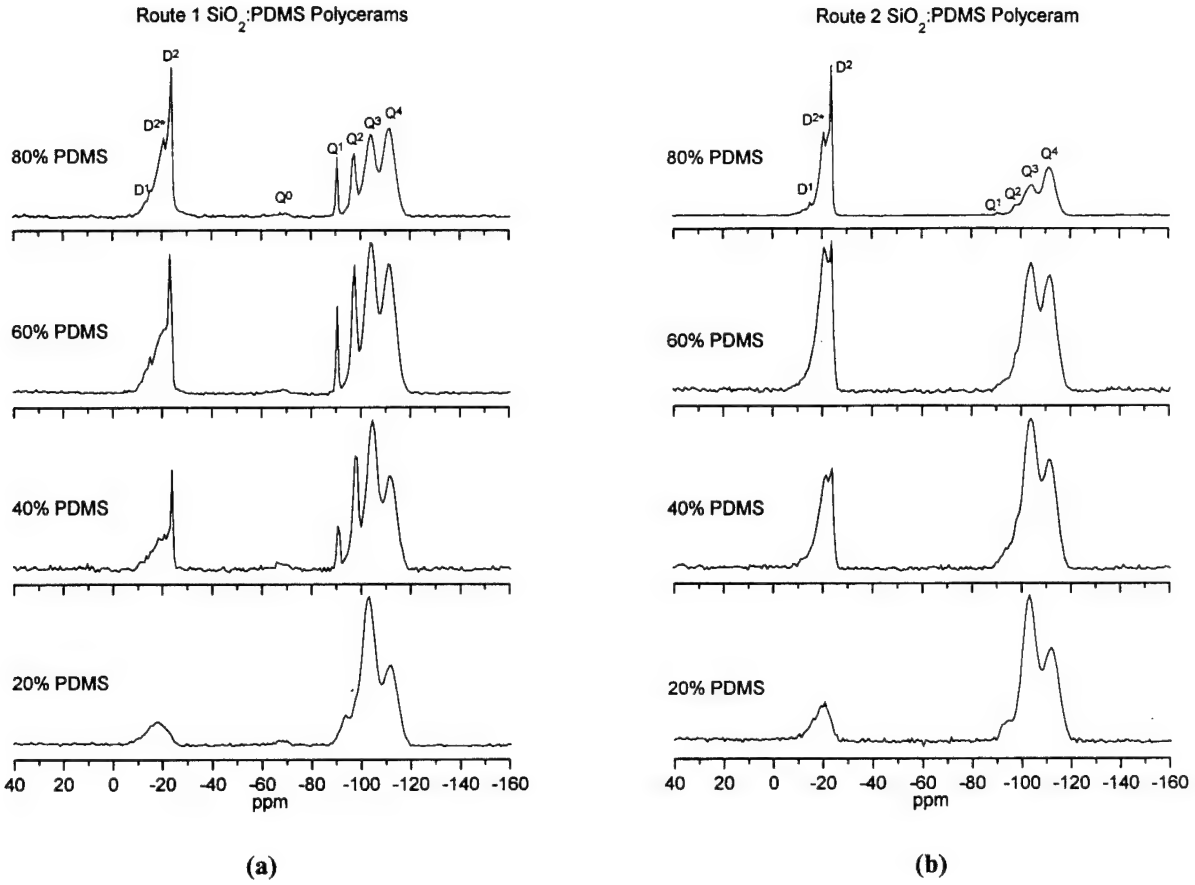

Figure 4: CP-MAS ^{29}Si NMR spectra for SiO_2:PDMS Polycerams with varying PDMS contents synthesized by (a) Route 1 and (b) Route 2.

The Route 2 Polyceram had a narrower co-condensation peak (D^{2*}) than the Route 1 Polyceram. The Route 1 Polyceram is more likely to have various D^2 species condensing with various Q species (D^2-Q^1, D^2-Q^2, D^2-Q^3, D^2-Q^4), while the D^2 species in the Route 2 Polycerams is more limited to co-condensation with Q^3 and Q^4 species (D^2-Q^3, D^2-Q^4) because there are few Q^1 and Q^2 species. Overall, the D^{2*} peak signifies that a large degree of co-condensation is occurring between the D and Q species, suggesting that organic and inorganic species are mixing close to the molecular level. The differences between the two Polycerams (Routes 1 and 2) is in the degree of crosslinking and the porosity.

3.2 Control of Porosity as a Function of Composition

Not only was the porosity controlled by variations in the synthetic route, but also by the PDMS content. Table 2 summarizes the properties of SiO_2:PDMS Polycerams synthesized by Routes 1 and 2 having various polymer contents. Figure 5a is a plot of the surface area of SiO_2:PDMS Polycerams synthesized by Routes 1 and 2 as a function of polymer content. The surface area of the 0 volume % PDMS sample synthesized by Route 2 was high at 573 m^2/gm. As the polymer content increased, the surface area and the porosity decreased, and reached zero at 60 volume % PDMS (Figure 5a). The pore size stayed essentially constant at about 40 Å. In contrast, the Route 1 Polycerams were all non-porous regardless of the polymer content.

The term 'non-porous' used in the present study represents a solid which is impermeable to N_2 molecules at 77K. That does not mean that these Polycerams are completely non-porous. First, the Polycerams may contain internal porosity which adsorption techniques cannot measure. Second, N_2 adsorption techniques cannot measure micropores (7 to 15 Å) and submicropores (< 7 Å), because these micropores are often not accessible to small molecules, such as N_2, at low

temperatures[4, 14]. Regardless of the faults of the quantitative nature of the N_2 adsorption measurements, the results demostrate that porosity can be varied dramatically with change in polymer content and processing route.

Table 2: Properties of SiO_2:PDMS Polycerams at various PDMS contents synthesized by Route 1 and Route 2.

Sample	Physical Properties	BET Surface Area (m^2/g)	Pore Size	Density (gm/cm^3)	Pore Volume (Volume Fraction pores)
Route 1 20% PDMS	non-syneresis drying, water resistant, hard	0.91	---	1.49 ±.01	0.00 (0.00)
Route 1 40% PDMS	non-syneresis drying, water resistant, hard	0.00	---	1.37 ±.01	0.00 (0.00)
Route 1 60% PDMS	non-syneresis drying, slow gelling, hard	0.00	---	1.31 ±.01	---
Route 1 80% PDMS	non-syneresis drying, slow gelling, soft	---	---	1.197	---
Route 2 0% PDMS	syneresis drying, brittle, very H_2O sensitive	573	42 Å	1.35 ±.01	0.59 cm^3/gm (0.79)
Route 2 20% PDMS	syneresis drying, brittle, H_2O sensitive	513	42 Å	1.124 ±.01	0.53 cm^3/gm (0.59)
Route 2 40% PDMS	syneresis drying, least tendency to crack, hard	342	39 Å	1.168 ±.01	0.33 cm^3/gm (0.38)
Route 2 60% PDMS	syneresis drying, hard	0.27	---	1.25 ±.01	0.001cm^3/gm (0.00)
Route 2 80% PDMS	less syneresis drying	---	---	1.22 ±.01	---

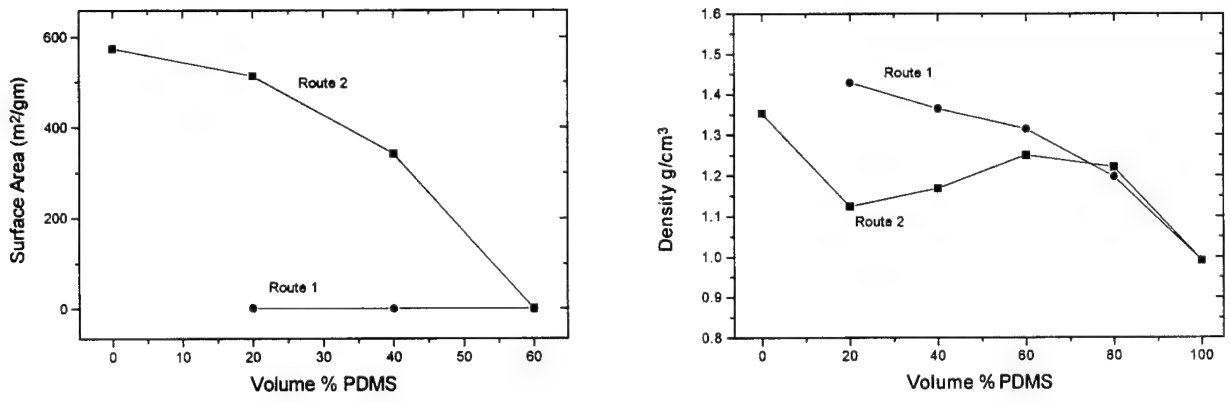

(a) **(b)**

Figure 5: (a) Surface area and (b) density of SiO_2:PDMS Polycerams synthesized by Routes 1 and 2 as function of the PDMS content.

The effect of polymer content on porosity and drying behavior with the Route 2 Polycerams can be associated with two phenomena: (1) the polymer "fills-in" the pores as the polymer content increases, thereby reducing the porosity; and (2) the silica condensation decreases as the polymer content increases due to co-condensation and steric hindrance. These phenomena are examined in the following discussion.

A more detailed look at the drying behavior of the Polycerams provides insights into possible structural changes as a function of polymer content. Two basic types of drying behavior were observed; syneresis and non-syneresis (Figure 2). For

syneresis drying to occur, one would expect the continuous matrix to be largely SiO_2 and not PDMS. In the range of 0-60% PDMS, syneresis drying behavior was observed with the Route 2 Polycerams but not with the Route 1 Polycerams. The Route 2 Polyceram at 60% PDMS was, however, also non-porous. If the reduction in porosity was caused solely by a decrease in the condensation, one would expect non-syneresis drying behavior with this sample. Instead, identical syneresis behavior (i.e., same radial shrinkage ($\Delta r/r$)) was observed with these Polycerams. The polypropylene beaker in which the Polyceram solutions were dried had a diameter of 2.2 cm, while the final monolith in the polymer content range of 0-60 % PDMS had a diameter of 1.0 cm. The height of these samples varied slightly, corresponding to measured densities of these samples. Because these samples shrank the same amount in the radial direction, this suggests that in the range of 0-60% PDMS the degree of silica condensation did not decrease dramatically and that the PDMS served effectively to "fill-in" the pores of the host matrix.

The "fill-in" idea would suggest that the inorganic framework is forming independently of the PDMS. However evaluation of the CP-MAS ^{29}Si data in Figure 4 gives strong evidence that there is a large amount of PDMS co-condensation and PDMS in Q environments due to the presence of the D^{2*} peak. The co-condensation of the PDMS could occur at the silica pore surface which would coincide with the "fill-in" model. The calculated pore volume required to "fill-up" all the silica pore surface in the 0% PDMS Route 2 Polyceram (surface area=573 m^2/gm), assuming the PDMS co-condenses to the silica pore surface at a cross-sectional area of 16 $Å^2$, is approximately 50-60 volume % PDMS. This back-of-the-envelope calculation corresponds well to observed surface area measurements in which the Polyceram becomes non-porous at 60% PDMS (Figure 5a), suggesting that it is possible for all the PDMS to co-condense at the silica pore surface. On the other hand, the co-condensation of PDMS could also result in the PDMS becoming a part of the continuous silica matrix, which would contribute to the decrease in the Q condensation due to steric hindrance of the PDMS. However for syneresis drying behavior to occur, it is likely that the continuous matrix is mostly inorganic with some co-condensation occurring within the inorganic framework, while most of the co-condensation occurs at the pore surface.

Further evidence supporting that PDMS is "filling-up" the pores as well as incorporating in the continuous silica matrix is suggested by the NMR Data (Figure 4b). At low PDMS contents (20% PDMS), the sharp D^2 peak is not observed, suggesting that almost all the PDMS oligomers are constrained in a silica environment (i.e., all the PDMS is in the continuous silica matrix and/or co-condensed at the pore surface). As the polymer content increased, the sharp D^2 peak becomes more pronounced. Hence more PDMS is occupying PDMS-rich regions or voids of the structure instead of occupying parts of the continuous silica matrix. At very high Polymer contents (80% PDMS), Q condensation appears to be significantly reduced. This is especially seen with the CP-MAS ^{29}Si NMR data with a significant increase in the Q^1 and Q^2 species relative to the Q^3 and Q^4 species of the Route 2 Polycerams from 60% PDMS to 80% PDMS (Figure 4b). Since the PDMS has occupied all the pores at 60% PDMS, further increase in the PDMS content disrupts more of the continuous silica matrix. Less syneresis drying (reflected by less shrinkage across the diameter and greater shrinkage across the height) of the 80% PDMS Polyceram (Route 2) compared to its 60% PDMS counterpart also supports this.

The location of the PDMS in the final structure is likely governed by competition of thermodynamic and kinetic driving forces. The driving force for the PDMS to go to the pores of the silica matrix may stem from large differences in the solubility parameters of PDMS (δ=8.16 $(cal/cm^3)^{1/2}$) and the silica surface (δ =13.39 $(cal/cm^3)^{1/2}$). The solubility parameters were calculated by summing up the group contributions of the cohesive energies and molar volumes[26]. The silica surface was represented by a partially reacted TEOS, where Si is bonded to one ethoxide group and one hydroxyl group. On the other hand, the PDMS is kinetically driven to be located in the continuous silica matrix due to the co-condensation reactions between the silica and PDMS.

If PDMS "fills-up" the pores of the matrix, then the size of the phase separation between the PDMS and silica matrix should be equivalent to the pore size. The pore size was small, ≈40 Å; therefore, the size of the phase separation should be ≈40 Å. For size comparison, the pore size is about the stretched length of only 3-4 PDMS oligomers.

The effect of PDMS content on the structure of the Route 1 Polycerams was different. Since the overall degree of condensation was low, the syneresis drying behavior did not occur and the materials were non-porous for all polymer contents. The PDMS cannot be drawn to the pores as in the Route 2 Polycerams. Therefore, it is believed that the PDMS addition to the Polyceram causes a more steric hindrance effect on the Q condensation. In Figure 4a, the Q^1 and Q^2 species increase noticeably with increase in PDMS content, reflecting the decrease in the Q condensation.

The densities of the Polycerams as a function of PDMS content and processing route shown in Figure 5b correlate well with the porosity measurements. The density of the Polycerams (ρ_t) can be described as:

$$\rho_t = V_{SiO2}\,\rho_{SiO2} + V_{PDMS}\,\rho_{PDMS} + V_{pore}\,\rho_{pore}$$

where ρ_{SiO2} is the skeletal density of the silica matrix, ρ_{PDMS} is the density of the PDMS polymer, ρ_{pore} is the density of the pore, V_{SiO2} is the volume fraction silica, V_{PDMS} is the volume fraction PDMS, and V_{pore} is the pore volume. The density of the polymer is 0.991 gm/cm^3 and the density of the air is 0.001 gm/cm^3. The theoretical skeletal density of silica has been reported as 2.05 gm/cm^3, although reported values for the skeletal density tend to vary depending on processing conditions (ranging from 1.88 to 2.19 gm/cm^3)[2]. Since all the Route 1 Polycerams were non-porous, the density decreased with increase in PDMS content because the density of PDMS is much less than the silica skeletal density. The Route 2 Polycerams were porous at PDMS contents less than 60%, and increases in the PDMS content up to 60% resulted in an increase in density, likely reflecting a "filling-up" of the voids in the structure. At higher PDMS contents (>60%), the Polycerams are non-porous, and the density decreases with increasing PDMS content (just as with the Route 1 Polycerams).

3.3 Structural Model and Photostability Case Study

The BET and NMR data on the SiO_2:PDMS Polycerams were used to produce 2D structural models to illustrate the concepts generated in the present study. These structural models are utilized as a case study for the specific application of laser dyes incorporated within Polyceram hosts. In previous studies performed in our laboratory, we doped a Pyrromethene laser dye within SiO_2:PDMS Polycerams to examine how the porosity and composition affect the photostability of the laser dyes[11, 12, 27]. The results indicated that photostability improved with decreasing porosity and increasing silica content. These photostability results on the Routes 1 and 2 Polycerams are correlated with the structural model.

The CP-MAS ^{29}Si NMR data in Figure 4 could not be used quantitatively to describe the ratio of the Q species. Because the cross polarization technique was used, there is an enhanced signal from silicate species located near hydrogen atoms. This allowed for investigation of the PDMS located in a constrained environment, but eliminated the possibility of evaluating the Q species quantitatively. Low Q species, such as Q^0, Q^1, and Q^2, had an enhanced response with respect to higher Q species (Q^3,Q^4), because the low Q species are more likely to have hydrogen atoms located near them. For this reason, the MAS ^{29}Si NMR measurements for some of the Polycerams were repeated without CP. The determined chemical shifts and the fraction of D or Q species are illustrated in Table 3.

Table 3: Chemical shifts ppm for SiO_2:PDMS Polycerams measured by MAS ^{29}Si NMR (No CP). Values in parentheses represent the fraction of Q^x species with respect to total amount of Q species present in the sample.

Sample	Q^0	Q^1	Q^2	Q^3	Q^4	Q^1:Q^2:Q^3:Q^4
20% PDMS Route 1	-67.3 (<.01)	-93.9 (.07)	-98 (.07)	-103.0 (.44)	-111.7 (.43)	1.0:1.0:6.3:6.1
40% PDMS Route 1	-67. (<.01)	-90.5 (.07)	-97.6 (.18)	-104.2 (.37)	-111.6 (.38)	1.0:2.6:5.3:5.4
20% PDMS Route 2	--- (.00)	≈-92 (.04)	≈-98 (.03)	-103.2 (.42)	-111.6 (.51)	1.0:0.8:10.5:12.8
40% PDMS Route 2	--- (.00)	-92.9 (.03)	-97.8 (.04)	-103.9 (.45)	-111.5 (.48)	1:1.3:15.0:16.0

In the proposed model, TEOS is represented by a "+" where the four ends correspond to the four functionality of TEOS, and the PDMS is represented by a thick curly line. The sizes of the species present in the Polycerams have been taken into account (1.2 Å for an O_2 molecule,1.6 Å for a Si-O-Si bond, 8-10 Å x 4 Å for a PDMS oligomer, and 13 Å x 6.4 Å for the PM-567 dye molecule). The dye concentration within a Polyceram is $5*10^{-5}$ M corresponding to $6*10^{17}$ cm^{-3} and an average dye-dye distance of about 120 Å. The oxygen concentration within PDMS will be used for the lack of a better value for the Polycerams, corresponding to $4.7*10^{18}$ cm^{-3} [28]. This results in an O_2:dye ratio of approximately 8:1. The oxygen molecules were randomly distributed in the structure, although there is a tendency for the O_2 molecules to be located at the pore surface[29, 30]. From the BET data, the average pore size and pore fraction were utilized (Table 2). For example, the 40% PDMS Polyceram synthesized by Route 2 has an average pore size of 42 Å and a open pore fraction of 0.38. It is assumed that the Polyceram also has microporosity and some closed porosity. Also, from the MAS ^{29}Si NMR data, the ratio of Q^1:Q^2:Q^3:Q^4 (Table 3) gives guidelines for connecting the "+" species to each other. The degree of PDMS condensation is high, based on the presence of the co-condensation D^{2*} NMR peak in Figure 4. For the 40% PDMS Polycerams the

SiO_2:PDMS ratio is 26:1 and for the 20% PDMS Polycerams the ratio is 76:1. Taking all these factors into account for each of the compositions described in Table 3, proposed structures for the SiO_2:PDMS Polycerams are shown in Figure 6.

The structural model illustrates a number of concepts discussed earlier in this paper. First, the Route 1 Polycerams are less condensed as seen by the greater number of Q^1 and Q^2 species (Figure 6a and 6c) compared to the Route 2 Polyceram (Figure 6b and 6d). Second, the Route 1 Polycerams do not have any external porosity, but do contain some microporosity and closed pores. Third, the porous nature of the material and the reduction in porosity with increase in polymer content of the Route 2 Polycerams are seen in the structural models. Finally, the structural models also illustrates how it is possible to have polymer co-condensed in the continuous silica matrix as well as have the remaining polymer 'filling-up" the small pores in the matrix. The ratios of the Q species define a set of boundary conditions on the structural model and imposes constraints on the structure of the silica matrix.

The structural model also helps illustrate why the photostability of the dye doped Polycerams is improved in non-porous and high silica Polycerams. It was determined in previous investigations that the Pyrromethene dye molecules degrades upon exposure to light by oxidation processes[12, 27]. Therefore the ability of oxygen to arrive at the dye molecules should determine whether the dye will react with oxygen. The model illustrates the large presence of oxygen in the Polyceram with respect to the dye and its easy access to the dye molecules located in the pores of the porous Polycerams (Figures 6b and 6d). The size of oxygen with respect to the pores is very small, and the diffusion of oxygen through the pores is likely very high. The structures for the 20% and 40% PDMS Polycerams synthesized by Route 1 (Figures 6a and 6c) portray a more difficult access of oxygen to the dye because of the non-porous nature of the material. In addition, the structure shows that the pores have varying degrees of accessibility for oxygen. The more porous the host material, the easier it is for oxygen to interact with the dye and undergo photochemical reaction to cause photodegradation. Photostability also improved with increasing SiO_2 content. The greater the SiO_2 content, the greater the chance of the dye to be caged due to the greater functionality of the SiO_2 (4 functional) compared to PDMS (2 functional). The improved photostability of the higher SiO_2 Polycerams also stems from the lower diffusivity of O_2 through dense SiO_2 versus PDMS[12, 28, 31, 32]. There is likely a distribution of dye molecules located within the pores and cages of the matrix, each dye molecule having a different probability of reacting with an oxygen molecule in a given time[12, 27].

CONCLUSIONS

Using two step acid/base sol-gel processes, a variety of optically transparent sol-gel monoliths have been synthesized. The control of the relative rates of condensation and evaporation as well as the polymer content made it possible to control the amount of porosity within the SiO_2:PDMS Polycerams ranging from materials with very high surface areas to materials which are essentially non-porous. These materials represent a new class of engineered porous materials. A structural model based on porosity measurements and ^{29}Si NMR data, correlates proposed structures to the physical properties and photostability characteristics of these materials.

ACKNOWLEDGEMENTS

The financial support of the Air Force Office of Scientific Research, the Corning Foundation Fellowship, and the Chapman Fellowship are gratefully acknowledged. The services of Kenner Christensen in performing the ^{29}Si NMR experiments is also acknowledged.

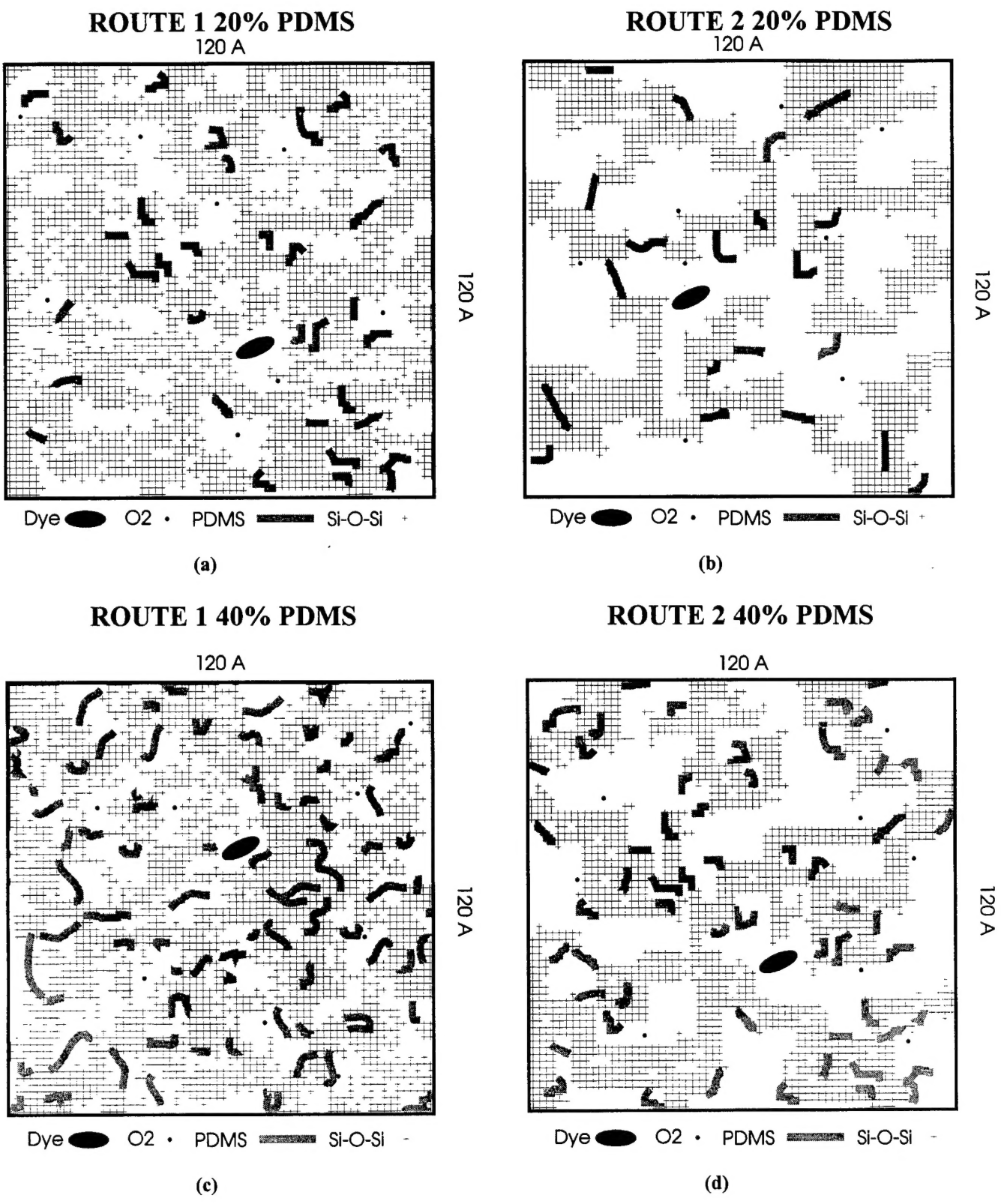

Figure 6: Proposed structures of SiO_2:PDMS Polycerams (a) at 20 vol % PDMS (Route 1), (b) at 20 vol % PDMS (Route 2), (c) at 40 vol % PDMS (Route 1), and (d) at 40 vol % PDMS (Route 2).

REFERENCES

1. D. W. Schaefer, *MRS Bulletin* **XIX**, 14-17 (1994).
2. C. Brinker, G. Scherer, *Sol-Gel Science* (Academic Press, Inc., Boston, 1990).
3. C. Brinker, S. Wallace, N. Raman, R. Sehgal, J. Samuel, S. Contakes, in *Access in Nanoporous Materials* T. Pinnavaia, M. Thorpe, Eds. (Plenum Press, New York, 1995) pp. 123-139.
4. F. Ehrburger-Dolle, J. Dallamano, G. Pajonk, E. Elaloui, in *Characterization of Porous Solids III* (1994), vol. 87, pp. 715-724.
5. L. Balducci, F. Montino, G. Cogliati, US Patent 5,270,027 (Istituto Guido Donegani, 1993).
6. M. McClain, D. Loy, S. Prabakar, in *Better Ceramics Through Chemistry VII: Organic/Inorganic Hybrid Materials* (MRS, 1996), vol. 435, pp. 277-282.
7. C. Guizard, P. Heckenbenner, J. Schrotter, N. Hovnanian, M. Smaihi, in *Better Ceramics Through Chemistry VII: Organic/Inorganic Hybrid Materials* . (MRS, 1996), vol. 435, pp. 283-294.
8. S. Kramer, F. Rubio-Alonso, J. D. Mackenzie, in *Better Ceramics Through Chemistry VII: Organic/Inorganic Hybrid Materials* (MRS, 1996), vol. 435, pp. 295-300.
9. L. Hench, in *Science of Ceramic Chemical Processing* D. R. Ulrich, L. Hench, Eds. (Wiley, New York, 1984) pp. 52.
10. S. Wallace, L. Hench, *Mat. Res. Soc. Symp. Proc.* **32**, 47 (1984).
11. T. Suratwala, Z. Gardlund, K. Davidson, D. R. Uhlmann, S. Bonilla, N. Peyghambarian, *Journal of Sol-Gel Science and Technology* **8**, 953-958 (1997).
12. T. Suratwala, Ph.D. Dissertation, University of Arizona (1996).
13. S. Lowell, *Introduction to Powder Surface Area* (John Wiley & Sons, New York, 1979).
14. I. Ismail, *Langmuir* **8**, 360-365 (1992).
15. C. Stock, E. Scofield, *Textile Research Journal* **July**, 521-526 (1951).
16. R. Iler, *The Chemistry of Silica* (John Wiley & Sons, New York, 1979).
17. R. Glaser, G. Wilkes, C. Bronnimann, *Journal of Non-Crystalline Solids* **113**, 73-87 (1989).
18. E. Lippmaa, M. Magi, A. Samoson, G. Engelhardt, A. Grimmer, *J. Am. Chem. Soc.* **102**, 4889 (1980).
19. G. Engelhardt, H. Jancke, E. Lippmaa, A. Samoson, *J. Organometallic Chem.* **210**, 295 (1981).
20. M. Magi, E. Lippmaa, A. Somoson, G. Engelhardt, A. Grimmer, *J. Phys. Chem.* **88**, 1518 (1984).
21. J. Kim, J. Plawsky, E. Wagenen, G. Korenowski, *Chem. Mater.* **5**, 1118-1125 (1993).
22. F. Babonneau, *New J. Chem.* **18**, 1065-1071 (1993).
23. F. Babonneau, *Mat. Res. Soc. Symp. Proc.* **346**, 949-960 (1994).
24. W. Klemperer, V. Mainz, D. Millar, *Mat. Res. Soc. Symp. Vol.* **73**, 15-25 (1986).
25. F. Babonneau, L. Bois, J. Livage, S. Dire, in *Nanophase and Nanocomposite Materials* S. Komarneni, J. Parker, G. Thomas, Eds. (MRS Symposium Proceedings, 1993), vol. 286, pp. 289-294.
26. D. W. VanKrevelen, *Properties of Polymers: Their Estimation and Correlation with Chemical Structure* (Elesevier Scientific Publishing Company, Amsterdam, 1976).
27. T. Suratwala, K. Davidson, Z. Gardlund, D. R. Uhlmann, S. Bonilla, N. Peyghambarian, *Solid State Lasers VI* **SPIE 2986**, 141-152 (1997).
28. B. Arkles, *Gelest Product Catalog* (1995).
29. A. Levy, D. Avnir, *J. Phys. Chem.* **97**, 10380-10384 (1993).
30. J. Samuel, M. Ottolenghi, D. Avnir, *Physica A* **191**, 153-167 (1992).
31. S. Pauly, in *Polymer Handbook* J. Brandrup, E. Immergut, Eds. (John Wiley & Sons, New York, 1989), vol. VI, pp. 435-449.
32. W. Kingery, H. Bowen, D. R. Uhlmann, *Introduction to Ceramics Second Edition* (John Wiley & Sons, New York, 1976).